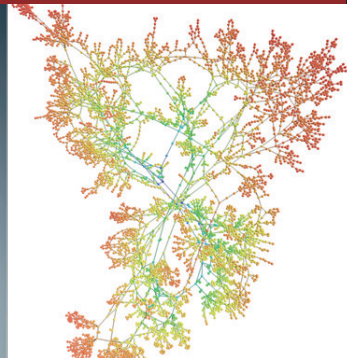
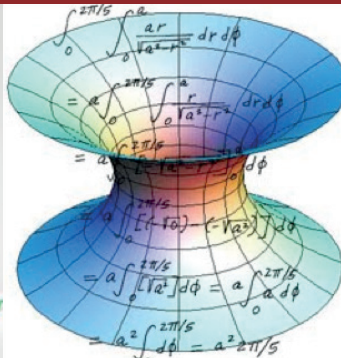


6TH URV DOCTORAL WORKSHOP IN COMPUTER SCIENCE AND MATHEMATICS

Edited by Carme Julià & Aïda Valls



UNIVERSITAT ROVIRA i VIRGILI

Title: 6th URV Doctoral Workshop in Computer Science and Mathematics
Editors: Carme Julià & Aïda Valls
April 2020

Universitat Rovira i Virgili
C/ de l'Escorxador, s/n
43003 – Tarragona
Catalunya (Spain)

ISBN: 978-84-8424-865-1
DOI: 10.17345/9788484248651

This work is licensed under the Creative Commons Attribution-NonCommercial-ShareAlike 4.0 International License. To view a copy of this license, visit <http://creativecommons.org/licenses/by-nc-sa/4.0/> or send a letter to Creative Commons, PO Box 1866, Mountain View, CA 94042, USA.

Preface

This book of proceedings gathers the contributions presented at the 6th URV Doctoral Workshop in Computer Science and Mathematics. This edition has been held in Tarragona (Catalonia, Spain) in 2020. It has been jointly organized by the research group Didactics of Mathematics (DIDACMAT) and the Doctoral Program on Computer Science and Mathematics of Security of Universitat Rovira i Virgili (URV). The main aim of this workshop is to promote the dissemination of the ideas, methods and results that are developed in the Doctoral Thesis of the students of this doctorate program, and to promote the knowledge, collaboration and discussion between their respective research groups.

The workshop had two invited talks, seven oral presentations and six posters. The first invited talk was given by Prof. Ernest Valveny, who is an associate professor at Universitat Autònoma de Barcelona and a researcher at Computer Vision Center; the talk revised the recent developments in text detection and recognition and explored the role of text in semantic image interpretation. The second invited talk was given by Prof. Virginia Larraz and Prof. Cèlia Baró, who are associate professors and researchers at Universitat d'Andorra. This talk presented the new educational model they designed and implemented in their University. This is an educational model completely based on the acquisition of a set of competences.

In this book, the reader will find the contributions of the thirteen Ph.D. students that presented their works in the Workshop. Each chapter presents the current research work of a doctoral student, the goals and some preliminary results. Contributions were framed in a variety of research lines, which include security and privacy in computer systems, artificial intelligence, medical informatics, hardware architectures, complex networks and mathematics. All contributions present innovative proposals, methods or applications, with the aim of opening new and strategic research lines. The editors and organizers invite you to contact the authors for more detailed explanations and encourage you to send them your suggestions and comments, which will certainly help them in their PhD theses.

The members of the organizing committee were Dr. Carme Julià, Dr. Aïda Valls (Coordinator of the Ph.D. program), Mr. Jaime Segarra, Mrs. Anna Santo and Mrs. Cristina Nieto. We would like to thank the invited speakers for such interesting talks. Second, we thank all the participants and, especially, the students that presented their work in this DCSM workshop. Finally, we also want to thank Universitat Rovira i Virgili (URV), the Departament d'Enginyeria Informàtica i Matemàtiques (DEIM) and the Escola Tècnica Superior d'Enginyeria (ETSE) for their support.

Dr. Carme Julià and Dr. Aïda Valls (Editors)

Contents

Cleaning, improving and validating the ICUs patients database in Hospital Joan XXIII for secondary use <i>David Cuadrado</i>	1
Optimizing CNNs first layer with respect to color encoding <i>João Paulo Schwarz Schüler</i>	5
State Support for Serverless Cloud Services <i>Daniel Barcelona-Pons</i>	9
Fairness in Federated Learning <i>Ashneet Khandpur Singh</i>	13
A Biomechanical Elastic Model for Estimation of Intra-Operative Complications Prostate Deformation <i>Muhamamd Qasim</i>	17
A Glance Of The Performance Potential of Serverless Computing <i>Ammar Mohammed Okran</i>	21
Quasi-ordinarization transform of a numerical semigroup <i>José Miguel Serradilla</i>	27
Secure total domination in rooted product graphs <i>Abel Cabrera Martínez</i>	31
Using The Feedback of Dynamic Active-Pixel Vision Sensor (Davis) to Prevent Slip in Real Time <i>Armin Masoumian</i>	35
A Human Assisted Model for Engineering Drawing Validation <i>Elena Rica</i>	41

Contents

The deployment of a decision support system for the diagnosis of Diabetic Retinopathy into a Catalan medical center <i>Emran Saleh, Najlaa Maarooof, Mohammed Jabreel</i>	45
Pre-service teachers' efficacy beliefs and attitude towards mathematics <i>Jaime Segarra Escandon</i>	49
Protecting Consumer Privacy in Smart Metering by Randomized Response <i>Bastian Stölb</i>	55

Cleaning, improving and validating the ICUs patients database in Hospital Joan XXIII for secondary use

David Cuadrado*

Department of Computer Engineering and Mathematics, Universitat Rovira i Virgili, Tarragona, Spain
david.cuadrado@estudiants.urv.cat

1 Introduction

The prediction of Days to discharge (DTD) is necessary for the proper management of an Intensive Care Unit (ICU), DTD predictions made by medical staff does not always are accurate [1]. Machine Learning could be used to create refined predictive models for DTD. The ICU of the Hospital Joan XXIII in Tarragona has an information system with data about all the admitted patients that combine data which is collected instantaneously with other data which is collected daily or once in the patient stay. A database with the information of patients in 2014-2019 was extracted and it is intended for obtaining DTD predictive models, but before that, it must first be debugged. This article describes the most relevant parts of the debugging process carried out, specifically the correction of erroneous values and the treatment of missing values.

2 Objective

The ICU database is extracted directly from the information system to ensure the anonymity of the patients for secondary use. Within the database, errors or missing values can affect the quality of the predicting models. The objective of this study is to obtain a debugged database by detecting and correcting erroneous values and reducing missing values.

3 Database description

The content of the database and its quality must be studied and classified before debugging.

* PhD advisor: David Riaño, Josep Gomez, Alejandro Rodriguez, Maria Bodí

3.1 Contents

The ICU database includes patients admitted in the ICU of the Hospital Joan XXIII during the 2014-2019 period. There are 5528 patients represented in 47192 days of total treatment. These patients have 47 attributes associated: PatientID, Age, Gender, DisYear (Age of discharge), PatType (Type of patient), AdmType (Type of admission), AdmWardGroup (Group of origin of admission), Outcome, PrevHospDays (Days in hospital before admission), APACHEAdmGroup (Group of admission APACHE), PrincipalDiagG (Main Diagnosis), TotalLOS (Total length of stay), APACHE-II (Patient Gravity Rating System), CHE (Patient Comorbidity), TSA (Time since admission), T2D (Time To Discharge), AE (External Factors), CA (Arterial Catheter), SU (Urinary Probe), CVC (Central Venous Catheter), Insuline, VA (Drugs vasoactive), SA (Sedoanalgesics), ATF (Antifungals), ATB (Antibiotics), VMI (Invasive Ventilation), VMNI (Non-invasive Ventilation), Isol (Isolation), LTSV (Life Support Limitation), MAP (Blood Pressure), HR (Heart Rate), Tmp (Temperature), Glu min, max and std (Minimum, Maximum glycemia and Standard deviation) NAS (Nursing Activity Score), EMINA (Pain scale), STRATIFY (Fall risk), SOFA (Gravity score of internal organs. There are 7 types), Data (Discharge request) and CAMICU (status of internal organs).

From the clinical point of view there are five types of attributes: Demographic (Age, Sex, Gender, ID, and DisYear), type of case (Patttype, Admtype, AdmWardGroup, APACHEAdmGroup, and PrincipalDiagG), clinical descriptions (CA, SU, CVC, Insuline, VA, SA, ATF, ATB, VMI, VMNI, Isol, LTSV, MAP, HR, Tmp, Glucose min, max, and standard deviation), scores (SOFAS, CHE, NAS, EMINA, STRATIFY, CAMICU, and APACHE-II) and organizational (PrevHospDays, TSA, LOS, T2D, and Outcome). Of these attributes there are 21 which are numerical, 12 categorical, and 14 binary. There are 14 attributes that contain data that is taken once at some point during the stay and 33 that are taken daily.

3.2 Quality of the original ICU database

In the original ICU database there are three types of error: erroneous values, impossible values, and anomalous values.

The erroneous values include 78 patients younger than 18 and 2 patient with unknown gender. There are also 37 patients registered as unknown type of patient.

The impossible values found include 121 patients with less than zero days in the hospital, prior to the admission in the ICU. There are also 925 days in which blood pressure is lower than zero.

The anomalous values involve three patients with an Admission Group tagged as zero, 791 patients with a length of stay longer than 14 days, and 172 patients with an APACHE score bigger than 37. The category AE (External

factors) is different to zero in only 1332 days, the Blood Pressure has values outside the range of [60,90] mmHg for 67 patients, and the Tmp has values outside the range of [33,44] °C in 8 days.

A missing value represents a data of the patient that has not been taken [2]. A first study allowed us to observe whether the missing values are concentrated in one year or if they are distributed over the years. All years have a similar proportion of missing values.

Missing values in the original database are concentrated in the next variables: MAP, HR, Tmp, Glu (min, max, std), NAS, EMINA, STRATIFY, CAMICU, and DATA. There are 105,809 missing values in the database.

4 Improving the database for secondary use

Erroneous and missing values received different treatments according to each case.

4.1 Detecting and correcting erroneous data

There are 78 patients younger than 18 and only one patient with unknown gender. They are removed from the database. For the 37 patients with PatType categorized as "Unknown", if the admission group was tagged as "Postoperative" or "Other non specific surgeries" the PatType was imputed as "Surgical", otherwise as "Medical".

The impossible negative values of the attribute PrevHospDays observed for 121 patients were set to zero. Negative blood pressure observed in 925 days for different patients were replaced with the values result from the interpolation between the days before and after. The three patients with an Admission Group tagged as zero were removed from the database. The attribute "LOS" (Length of stay) is useless for DTD analysis, therefore it is removed.

4.2 Reducing missing values

Missing values are distributed along the 2014-19 years with percentages 4.89 %, 4.96 %, 5.11 %, 5.32 %, 4.56 %, and 3.82 %. Only 11 attributes contain missing values, and only two of them (CAMICU, Data) register 86.32 % and 99.98 % of missing data, respectively. They were removed. CAMICU and Data attributes were also removed due to the huge amount of missing values. The other attributes have less than 4 % missing values, except NAS that has 12.74 %. They are kept and their missing values are imputed. Two imputation mechanisms were used: interpolation and replication.

If the value of an attribute is missing but known in the days before and after (for a patient), these last two values were averaged and the result used to replace the missing value in the intermediate day. If only one of the values

in the day before or after is known, it is replicated in the intermediate missing value.

5 Results and future work

In the debugging process, we eliminated four attributes (LOS, AE, CAM-ICU, and Data), we introduced 425 new missing values, corresponding to 124 patients, but we also corrected a considerable number of erroneous values (2110 values corresponding to 172 patients). Table 1 shows the compared number of days, patients, attributes, and missing data in the UCI database before and after our debugging.

	Previous	Final
N (days)=	47192	46684
N (patients)=	5529	5445
N attributes=	47	43
N missing=	105809	17623
% missing=	4.77 %	0.88%

Table 1: Days, patients, attributes, and missing data in the UCI database

Some attributes such as MAP, AE, and Tmp may require a more refined debugging that could potentially improve the current results. In the future, this work will allow us to apply machine learning methods to extract models to predict DTD of patients in an ICU to improve the current prediction of practitioners.

References

- [1] Cuadrado D., Riaño D., Wilk S., ten Teije A. *Pursuing Optimal Prediction of Discharge Time in ICUs with Machine Learning Methods*. Artificial Intelligence in Medicine. AIME 2019. Lecture Notes in Computer Science, vol 11526. Springer, Cham.
- [2] I. Ezzine and L. Benhlima. *A Study of Handling Missing Data Methods for Big Data*. 2018 IEEE 5th International Congress on Information Science and Technology (CiSt), Marrakech, 2018, pp. 498-501.
- [3] Liu YN, Li JZ, Zou ZN. *Determining the real data completeness of a relational dataset*. Journal of computer science and technology 31(4): 720–740 July 2016. DOI 10.1007/s11390-016-1659-x.

Optimizing CNNs first layer with respect to color encoding

João Paulo Schwarz Schüler *

Department of Computer Engineering and Mathematics, Universitat Rovira i Virgili
Tarragona, Spain

joaopaulo.schwarz@estudiants.urv.cat

1 Introduction

In 1989, LeCun et al. [7] devised the first Convolutional Neural Network (CNN), which mimicked the organization of neural cells in the visual cortex as convolutional filters. This new type of neural network was able to recognize 10 digits in hand-written text very accurately. The majority of existing CNN models deal with the basic Red-Green-Blue (RGB) color values from input pixels. Despite this is the obvious choice taking into account that digital images are usually encoded with RGB, it's curious that very few researchers have attempted to train their networks on images encoded with other color spaces such as Hue-Saturation-Lightness (HSL) or CIE-LAB, the definition of which are vastly known and long-standing in the fields of color perception [2] and colorimetry [6]. The rationale behind trying other color spaces than RGB is based on evidences that the human color vision transforms the initial neural signals from cones and rods into an opponent color model [5], where several layers of neurons convert the Short, Medium and Large wavelength neural signals, loosely related to blue, green and red hues, into other neural signals. In regards to the human color perception [2], these opponent signals are further processed and converted into perceptual color components, named as Hue, Saturation and Lightness. There are several computational models that convert RGB into HSL-related components, for example, Smith's HSI [3] and Yagi's HSV [4].

2 Materials and methods

In order to check our hypothesis, we will perform image classification experiments on the CIFAR-10 dataset [1], which consists of 60k 32x32 RGB labelled images, belonging to 10 different classes: airplane, automobile, bird, cat, etc. These images are taken from natural and uncontrolled lightning environment,

* PhD advisors: Domènec Puig, Santiago Romani and Mohamed Abdel-Nasser

contain only one prominent instance of the object to which the class refers, and the object may be partially occluded or seen from an unusual viewpoint. We aim to explore the simplest CNN able to obtain a reasonable test accuracy (above 80%) in the CIFAR-10 image classification task, in order to compare its behavior (accuracy variation, patterns in first layer filter, etc.) with various color encodings, from the basic RGB to HSL or LAB, as well as the bare gray level value of pixels (colorless images).

3 Experiments

As a baseline, we defined a single-branch CNN architecture small enough to classify CIFAR-10 dataset with at least 80% test accuracy. This single-branch architecture is shown in figure 1.

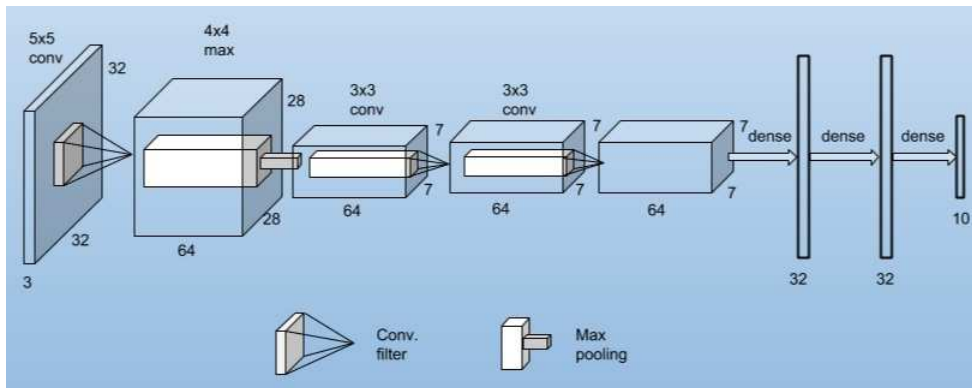


Fig. 1: Graphical representation of the single-branch baseline CNN architecture.

One of the purposes of our research is to create an architecture that takes advantage of separated chromatic and achromatic channels, which are readily available in color spaces such as CIE-LAB or HSV, as explained in the introductory section. To this aim, we propose to create two separate paths for the first convolutional layer, each one dedicated to each type of pixel information (achromatic/chromatic), in order to specialize the first layer filters of the CNN to the mentioned aspects of the scene (light variations, object boundaries). We hypothesize that this specialization may lead to better object identification, as a consequence of a more object-related representation of the image content. Figure 2 shows the proposed two-branch architecture, where the top branch processes the single achromatic channel while the bottom branch processes the two chromatic channels. For example, we can convert RGB into CIE-LAB

color encoding, hence the L channel is fed into the top branch, while the AB channels are fed into the bottom branch.

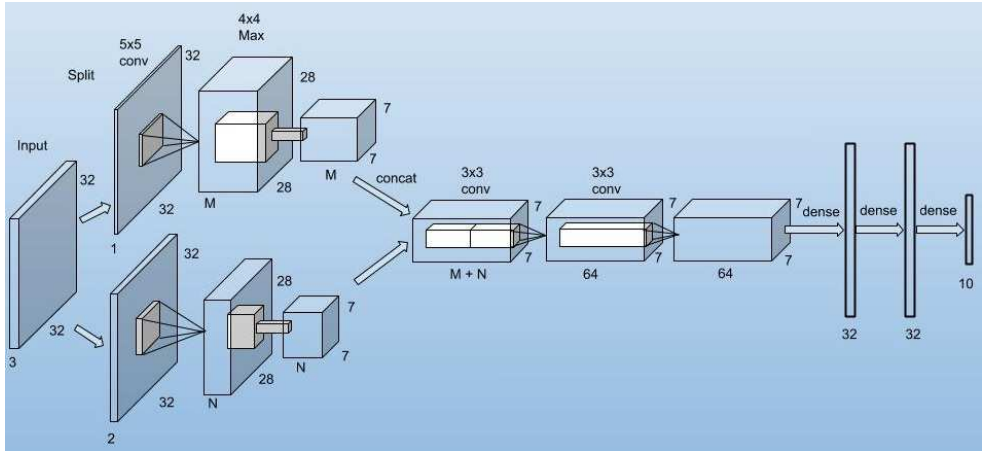


Fig. 2: Graphical representation of the single-branch baseline CNN architecture.

4 Results

As shown in the table 1, our baseline RGB model obtained 84.4% accuracy with 15.5 million floating point operations on the forward pass while our two-paths model obtained 84.7% accuracy with 11.7 million flops meaning a reduction about 29% in the required forward pass computation.

model	color space	accuracy	million flops
baseline	RGB	84.4%	16.5
two-paths	LAB	84.7%	11.7

Table 1: RGB baseline and LAB two-paths results.

5 Conclusions

By splitting LAB filter values into two branches, one for L and another for AB, we can force a CNN to find prototypical sets of achromatic/chromatic filters allowing the CNN to achieve similar accuracy while decreasing the required computation. In essence, we have devised a modification of the first

layer of a CNN into two branches, which optimizes the number of weights when dealing with a color encoding that separates achromatic from chromatic channels, such as LAB, HSL, etc. Although the proposed architecture does not increase the validation accuracy significantly, it points out that uncorrelating the input features eases the learning task of any CNN. As a future work in this line, we aim to find out other “correlations” in mid-level or high-level layers, hence we may be able to specialize the network neurons to different types of information.

References

- [1] A. Krizhevsky, G. Hinton. Learning Multiple Layers of Features from Tiny Images. 2009. doi:10.1.1.222.9220.
- [2] A.R. Robertson. Color Perception. *Phys. Today.*, 45 (1992) 24–29. doi:10.1063/1.881324.
- [3] A.R. Smith. Color Gamut Transform Pairs. *SIGGRAPH Comput. Graph.*, 12 (1978) 12–19. doi:10.1145/965139.807361.
- [4] D. Yagi, K. Abe, H. Nakatani Segmentation of Color Aerial Photographs Using HSV Color Models. *Proc. IAPR Work. Mach. Vis. Appl. MVA*, December December 7-9, 1992, Tokyo, Japan, 1992: pp. 367–370. <http://b2.cvl.iis.u-tokyo.ac.jp/mva/proceedings/CommemorativeDVD/1992/papers/1992367.pdf>.
- [5] E. Hering Outlines of a Theory of the Light Sense. *Harvard University Press*, 1920.
- [6] G. Wyszecki, W. S. Stiles. Color Science: Concepts and Methods, Quantitative Data and Formulae, 2nd Edition *Color Sci. Concepts Methods, Quant. Data Formulae, 2nd Ed.*, Pp. 968. ISBN 0-471-39918-3. Wiley-VCH , July 2000. (2000). 2007.
- [7] Y. LeCun, B. Boser, J.S. Denker, D. Henderson, R.E. Howard, W. Hubbard, L.D. Jackel Backpropagation Applied to Handwritten Zip Code Recognition *Neural Comput.*, 1 (1989) 541–551.

State Support for Serverless Cloud Services

Daniel Barcelona-Pons *

Department of Computer Engineering and Mathematics, Universitat Rovira i Virgili
Tarragona, Spain
daniel.barcelona@urv.cat

1 Serverless

The cloud has been a hot topic in recent years for both, industry and academia. Captivated by the simplification, cost reduction, and other benefits of cloud services, many companies have moved their applications and services to managed infrastructure in the cloud. The most relevant offerings are provided by Amazon, Microsoft, Google, and IBM. The advantage of this model is the increasing level of abstraction the user faces (IaaS, CaaS, PaaS). With the each time more reduced complexity, more sectors have available the cloud's compute capacity.

However, the cloud is still evolving. The latest development in this line is *serverless*. This new model establishes a philosophy where a cloud service user is totally oblivious to the servers. That way, they do not need to worry about provisioning and managing servers and can focus on their applications. Another important property of serverless is its billing model. In a serverless service, the user is only charged for the exact resources they use, at very fine granularity (in the order of milliseconds and few megabytes). This allows users to pay only for the performance required at any particular moment, against paying for machines working all day—thus, avoiding charges for idle resources.

The serverless model importantly emerged in 2014, with AWS Lambda [1]. This service establishes the basis of what is the most popular compute offering in the serverless world: Function as a Service (FaaS). Academia quickly started to analyze this model and examine its potential and limitations [2]. In this system, the user codes functions; small pieces of code with clearly defined functionality, some input parameters and some output. The functions are deployed directly to the cloud and are run as response to events, on demand. Additionally, functions execute in isolated environments (containers, e.g. Docker), and after running, the environment disappears. This makes each execution independent of the resources it is actually running on, allowing creating a new environment with the function for each event or invocation, hence

* PhD advisor: Pedro García-López

making the service highly scalable. As a serverless service, it allows a user to quickly execute code in the cloud by just providing it and triggering it, without needing to configure or manage any of the underlying resources, which are managed transparently by the cloud provider. Following the appearance of Amazon’s service, other cloud providers like Microsoft, Google, and IBM presented their counterparts: Azure functions, Google Cloud Functions, and IBM Cloud functions. Each of those have their own characteristics and limitations, but they all follow the same FaaS scheme.

FaaS is the main component of serverless computing, and usually confused with serverless in general. However, it is just a way of offering computation by following the serverless philosophy. For instance, serverless can also be applied to storage. There are storage services in the cloud, like Amazon S3 and DynamoDB, that also offer pay-per-use with zero server management.

1.1 Current state and open challenges

Serverless, and more specifically FaaS, is a very good fit for many kinds of applications, e.g. web services and backend. We have seen them used to serve websites, or as substrate for web applications, as well as for authorization procedures. We have also examples of functions being used for background processes, like resizing uploaded images, or scheduled maintenance jobs. And they can be used for more interactive tasks too, like real time translations.

Nonetheless, it is a new model still in evolution and its offer is not complete yet (cloud providers still add new features and tune their services [8] and there is a lot of academic movement [4,6,7,5] exploring the limits of the model). This early state of the model makes many applications face several issues when trying to benefit from it. Such applications include data analytics in Big Data, machine learning (ML) training, algebra and graph computations. Implementing them is either not possible or highly inefficient with the current serverless offer, but however desirable for many data scientists to scale their computations with ease in the cloud. This is mainly due to two limitations in the FaaS model, consequence of their ephemeral nature (functions are expected to run a simple task and return quickly, hence they having a tiny time limit—up to 15 minutes).

First, function executions are ephemeral: stateless and non-addressable; they cannot store any kind of state between function invocations, since each one could run on different environments; and function invocations cannot be reached by other processes since they do not expose any endpoint. This thwarts the logic capabilities of functions and the implementation of iterative tasks that need to work continuously with the same data (e.g., ML training over a data set). Developers are forced to use external services to store their data reliably and allow sharing some state between functions to scale a computation. Unfortunately, current cloud storage services are not prepared to deal with this kind of workload, where rapid access and bandwidth are very important. Serverless

storage services like object stores are too slow for fine-grained state sharing, and in-memory stores are not prepared for the scale FaaS is able to achieve. Second, FaaS services do not provide means to coordinate and synchronize function executions. This is related to the fact that functions are not addressable. We have seen projects that see FaaS as an infinite computation cluster, where each function is a compute unit (e.g., PyWren [6] and ExCamera [4]). For this model to work, functions need to coordinate. Having information and being able to react when each of the tasks finishes, know when to run new ones, and create operation workflows, is an important requirement for such distributed applications to be developed easily in a serverless way. Currently, this is not directly supported in FaaS services and it is required to use external controllers with certain limitations: functions need to be called synchronously, by blocking the client, and data and results must be obtained by polling external storage; Due to this lack of integrated support, coordination cannot benefit from internal events to make orchestrations more automatic, reactive and scalable. Several orchestration services have appeared, like AWS Step Functions, IBM Composer, and Azure Durable Functions, but they do not fulfill the requirements for fully reactive workflow management [5]. Recently, an extended discussion about serverless and its challenges (including the ones discussed here) has been published [7].

The research presented in this document chases these challenges.

2 Serverless stateful computation

This section gives a quick description of the current work performed to solve these challenges and that will be part of the PhD thesis.

As a first step towards enabling highly-concurrent stateful computation for FaaS services, we designed Crucial. Its simple programming model allows to port effortlessly multi-threaded algorithms to serverless. Crucial is built upon the key insight that FaaS resembles to concurrent programming at the scale of a data center. Then, to share state at fine granularity and enable coordination between functions, a distributed shared memory layer is the right answer. Figure 1 shows the general architecture of the system, where we see how FaaS functions are considered traditional threads (run from a client application) and they all have access to the same in-memory store to share state. The first results of this work have been published recently [3].

Acknowledgement. Daniel Barcelona-Pons’s work is financed by a Martí i Franquès Programme grant (URV). This work has been partially supported by the EU Horizon 2020 programme under grant agreement No 825184 and by the Spanish Government through project TIN2016-77836-C2-1-R.

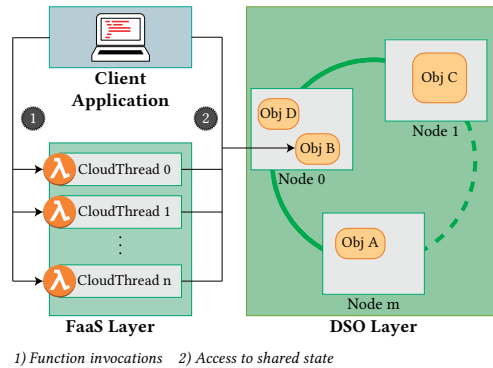


Fig. 1: A client application runs a set of threads on the FaaS layer; all of them have access to the same shared state at the distributed shared object (DSO) layer.

References

- [1] Amazon. AWS Lambda. <https://docs.aws.amazon.com/lambda>, 2014.
- [2] I. Baldini, P. Castro, K. Chang, P. Cheng, S. Fink, V. Ishakian, N. Mitchell, V. Muthusamy, R. Rabbah, A. Slominski and P. Suter. Serverless Computing: Current Trends and Open Problems. *Research Advances in Cloud Computing, Singapore*, pp. 1-20, 2017.
- [3] D. Barcelona-Pons, M. Sánchez-Artigas, G. París, P. Sutra, and P. García-López. On the FaaS Track: Building Stateful Distributed Applications with Serverless Architectures. *Proceedings of the 20th International Middleware Conference (Middleware '19)*, pp. 41–54, 2019.
- [4] S. Fouladi, R. S. Wahby, B. Shacklett, K. V. Balasubramaniam, W. Zeng, R. Bhalerao, A. Sivaraman, G. Porter and K. Winstein. Encoding, Fast and Slow: Low-Latency Video Processing Using Thousands of Tiny Threads. *14th USENIX Symposium on Networked Systems Design and Implementation (NSDI'17)*, 2017.
- [5] P. García-López, M. Sánchez-Artigas, G. París, D. Barcelona-Pons, Á. Ruiz-Ollobarren, and D. Arroyo-Pinto. Comparison of FaaS Orchestration Systems. *2018 IEEE/ACM International Conference on Utility and Cloud Computing Companion (UCC Companion)*. IEEE, pp. 148–153, 2018.
- [6] E. Jonas, Q. Pu, S. Venkataraman, I. Stoica and B. Recht. Occupy the Cloud: Distributed Computing for the 99%. *Proceedings of the 2017 Symposium on Cloud Computing*, 2017.
- [7] E. Jonas, J. Schleier-Smith, V. Sreekanti, C.-C. Tsai, A. Khandelwal, Q. Pu, V. Shankar, J. Menezes Carreira, K. Krauth, N. Yadwadkar, J. Gonzalez, R. A. Popa, I. Stoica and D. A. Patterson. Cloud Programming Simplified: A Berkeley View on Serverless Computing. EECS Department, University of California, Berkeley, Berkeley, 2019.
- [8] Serverless blog. All the Serverless announcements at re:Invent 2019.

Fairness in Federated Learning

Ashneet Khandpur Singh *

Department of Computer Engineering and Mathematics, Universitat Rovira i Virgili
Tarragona, Spain
ashneet.singh@urv.cat

1 Introduction

The advancements of machine learning in the current world are taking place in our daily lives: from music suggestions made from our playback history to the automotive industry [1]. These technologies have access to individual's data for learning models, often in privacy-invasive ways, which causes a break to these technological advances. In order for the progress of this technology to be built efficiently, it is necessary to consider a balance between the technological advances and the usage of individual's data. An alternative approach to machine learning, called decentralized federated learning [2,3], is hereby considered where data is not collected, i.e. it leaves the training data distributed on the mobile devices and learns a shared model by aggregating locally-computed updates.

In federated learning, a centrally located server sends a model to user devices, also known as clients, which can be in the range from hundreds to millions depending on the user base of the application. Each client downloads the current model, improves it by learning from data on their respective device, and then summarizes the changes as a small focused update. All clients send their updates to the central server, using encrypted communication, where it is averaged with other user updates to improve the shared model. The new shared model is sent back to the devices and this cycle iterates until the model is improved. Federated learning enables sharing information between a client and server without compromising on user privacy.

The algorithms in federated learning may use a central server that orchestrates the different steps of the algorithm and acts as a reference clock, or they may be peer-to-peer, where no such central server exists.

* PhD advisor: Josep Domingo-Ferrer

1.1 Current research

With the increasing usage of machine learning techniques that rely heavily on data, there is a need to ensure fair practices that do not propagate biases. Fairness matters because it has impact on everyone's benefit.

The data provided by the mobile devices can be highly biased. If the training data coming from some minority group is much less than those coming from a majority group, it is less likely to model perfectly the minority group. To prevent clients from minority groups to contribute to the learning process, which therefore yields models built on the data on the non-minority clients, we need to discard updates that differ too much from the rest. On the other hand, malicious attacks aiming at poisoning the learned model are also likely to provide updates that differ very much from the mainstream. For that, we propose two different solutions to distinguish poisoners from genuine outliers/minority group members.

1. The first one is based on microaggregation [4], which attempts to create clusters such that the published attributes of the genuine outliers in each cluster are maximally similar.
2. The second solution is based on Gaussian Mixtures.

These two proposals were implemented using Python and evaluated on the Adult data set obtained from the UCI Machine Learning repository [7]. We created three different kind of participants in the Adult data set, where one of them were cheaters. By including diverse clients, we strive to help learning less discriminatory machine learning models. For the first solution, we used the maximum distance to average vector (MDAV) algorithm, with which we were able to differentiate the cheaters from the rest of the participants. In the second solution, the expectation-maximization (EM) algorithm [5,6] has been employed and is currently under work.

Acknowledgement. Partial support to this work has been received from the European Commission (project H2020-871042 "SoBigData++"), the Government of Catalonia (ICREA Acadèmia Prize to J. Domingo-Ferrer and grant 2017 SGR 705), and from the Spanish Government (project RTI2018-095094-B-C21 "Consent" and TIN2016-80250-R Sec-MCloud). The authors are with the UNESCO Chair in Data Privacy, but the views in this paper are their own and are not necessarily shared by UNESCO.

References

- [1] Stilgoe, J. Machine learning, social learning and the governance of self-driving cars. *Social studies of science*, 48(1), 25-56, 2018.
- [2] McMahan, H. B., Ramage, D. Federated learning: Collaborative machine learning without centralized training data.

<https://research.googleblog.com/2017/04/federated-learning-collaborative.html>, 2017.

- [3] McMahan, H. B., Moore, E., Ramage, D., Hampson, S. Communication-efficient learning of deep networks from decentralized data *arXiv preprint arXiv:1602.05629,2016*
- [4] J. Domingo-Ferrer, V. Torra. Ordinal, continuous and heterogeneous k -anonymity through microaggregation. *Data Mining and Knowledge Discovery* 11(2) (2005) 195-212.
- [5] Redner, R. A., Walker, H. F. Mixture densities, maximum likelihood and the EM algorithm. *SIAM review*, 26(2), 195-239, 1984.
- [6] Roche, A. EM algorithm and variants: An informal tutorial. *arXiv preprint arXiv:1105.1476*, 2011
- [7] C. Blake and C. Merz. *UCI repository of machine learning databases*, 1998.

A Biomechanical Elastic Model for Estimation of Intra-Operative Complications Prostate Deformation

Muhamamd Qasim *

Department of Computer Engineering and Mathematics, Universitat Rovira i Virgili
Tarragona, Spain
muhammad.qasim@urv.cat

1 Introduction

Cancer sets up a massive burden on societies throughout the world and prostate cancer (PCa) is one of the most noncutaneous cancer in men and the second leading cause of death worldwide [1]. In spite of its small size, PCa grows in the peripheral zone of the gland and can extend to a significant length before involving male genitourinary system [2].

On account of the elastic properties of soft tissues, doctors routinely use palpation to distinguish lesions within the prostate. Because, cancerous tissues are more rigid than normal tissues [3]. However, manual palpation is difficult for the inside lesions when the elasticity values are similar between the tissues. In addition, it does not provide any statistical or numerical information, and the effectiveness depends on the skill and experience of the surgeons. Therefore, ultrasound-based elasticity-imaging methods and other elastography methods were developed to overcome those limitations.

Patient-specific modeling is very crucial for successful diagnoses of cancer and treatments because of the dependence on the patient's material properties of the tissues, geometry, etc. For example, Wang et al. [4] focused on patient-specific biomechanical parameters for inner and outer prostate tissue by employing shear wave elastography and proposed a deformation model for estimating patient-specific prostate deformation during image-guided interventions.

Currently, transrectal ultrasound (TRUS) is used in the routine clinical practice for targeting the prostate lesions because it is safe and affordable but specialists are facing some challenges when performing TRUS-guided biopsy. One of them is how to track the location of prostate lesions, given the pressure of TRUS at the rectum side (see fig. 1: Pressure Face) and also have the deformation of the prostate and surrounding areas. Second of them is how to

* PhD advisor: Carme Olivé , Dolors Puigjaner, Joan Herrero, Josep M. López, Gerard Fortuny

fit the appropriate parameters of rectum, bladder, pelvic bones and especially for prostate tissues for realistic deformation model.

2 Methodology and Results

Three-dimensional finite element (FE) pelvis organs are constructed to delineate the effect of different organ geometries as shown in Figure 1. The simulations are done in Code_Aster [5] open source software to see the elastic biomechanical behavior of pelvic organs. The surfaces of rectum, bladder and pelvic bones are discretized with linear thin-triangular shell elements while 3D four-node tetrahedral voluminal elements are used for the inner and outer prostate. Kinematic boundary conditions are examined for sacrum and hips in terms of node displacements i.e. ($U_x = 0$, $U_y = 0$ and $U_z = 0$). As stated above, the transrectal ultrasound (TRUS) guided biopsy is used to target the prostate lesion by applying pressure on one side of rectum. The Doctor presses with a transducer to locate the prostate and the regions with injury. A similar condition this work, real properties are used for all tissues in the region (including injured tissue). Then a pressure similar to that practiced by the doctor in the biopsy is practiced on the part of the inside of the rectum (Figure 1: Pressure face).

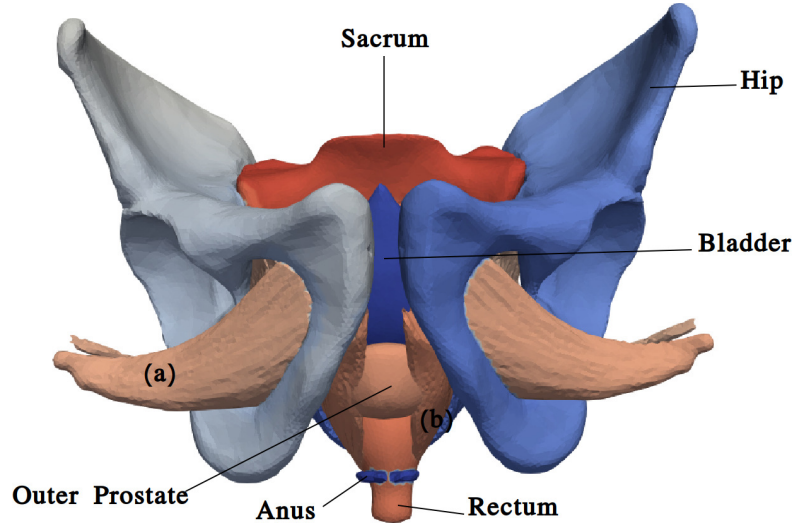


Fig. 1: 3-D pelvis system, organs a, b and among others are soft tissues.

Figure 2 shows the displacements obtained, the behavior of linear-elastic deformation after establishing the biomechanical parameters for each organ.

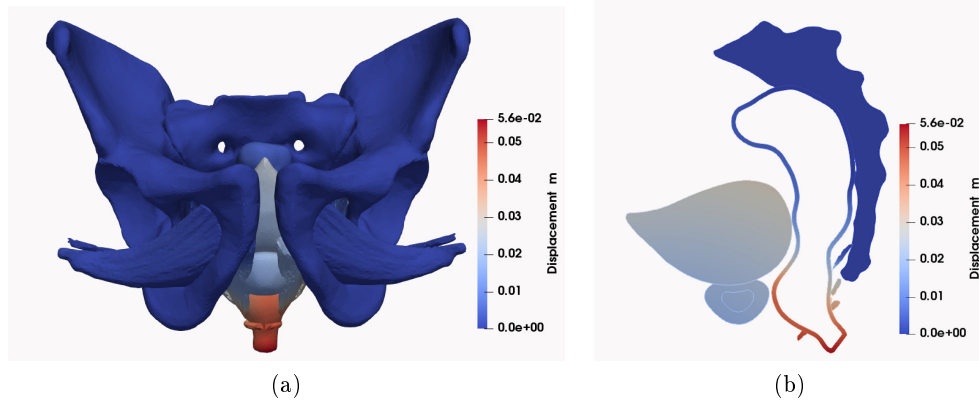


Fig. 2: (a) Frontal and lateral view (b) with displacements values.

3 Conclusions

The present methodology allowed us to greatly improve the location of prostate motion during TRUS procedure. Because we can estimate with great precision the final location of the lesions observed during the Computerized Axial Tomography. The correct location of the lesions will allow biopsies of damaged tissues, so as to avoid false negatives in patients.

Acknowledgement. This work was partially supported by grant No. 713679 from the European Union's Horizon 2020 Research and Innovation Programme under the Marie Skłodowska-Curie grant agreement and from Martí i Franquès COFUND Fellowship Programme from Universitat Rovira i Virgili.

References

- [1] Lindsey A., Torre, Freddie Bray, Rebecca L., Siegel, Jacques Ferlay, Joannie Lortet-Tieulent, Ahmedin Jemal. *Cancer statistics*. CA Cancer J Clin., 65: 87–108, 2015.
- [2] Wein AJ, Kavoussi LR, Novick AC, Partin AW, Peters CA. *Campbell-Walsh Urology*. Elsevier Saunders, Philadelphia, 2012.
- [3] W. A. D. Anderson. *Pathology*. The C. V. Mosby Co, St. Louis, MO, 1953.
- [4] Yi Wang, Dong Ni, Jing Qin, Ming Xu, Xiaoyan Xie, Pheng-Ann Heng. *Patient-specific deformation modelling via elastography: application to image-guided prostate interventions*. Scientific Reports, 27386:6, 2016.
- [5] Aster. *Electricité de France, Finite element code aster, Analysis of Structures and Thermodynamics for Studies and Research*, 1989-2017. 1989-2017. <https://www.code-aster.org/>

A Glance Of The Performance Potential of Serverless Computing

Ammar Mohammed Okran *

Department of Computer Engineering and Mathematics, URV, Tarragona, Spain
ammар.okran@urv.cat

1 Introduction

Cloud computing, also known as "Serverless Computing", has become widely popular during the recent years and it has already gained a large amount of users as they can access to a large pool of services (such as storage, computing power or applications) over the internet avoiding the complexity and cost of maintaining their own infrastructure. These resources are provided on demand and the payment is made according to the amount of use. One of the advantages of cloud computing is that it facilitates the issue of the resources in many aspects as the users can store and access data online whenever they want and wherever they are, with no need to their computer's hard drive. This means that data is stored in a remote place and it could be accessed from anywhere. Cloud service providers such as Google, Microsoft, Amazon or IBM are racing in order to provide a good service to the potential users. All of them are well aware that this guarantees to continue and compete in the market and attract a lot of customers. However, this can only be done through the simplicity, elasticity, and performance efficiency of services.

To do this, we will perform several experiments using the services provided by the IBM cloud platform, executing an algorithm that works with LIDAR data and categorizing all the times involved from the beginning to the end of each experiment. The results obtained will give us a clearer vision of the potential performance of this platform and will help us identify possible areas for improvement.

2 IBM Cloud

IBM cloud is a range of cloud computing services provided by the IBM company and it includes platform as a service (PaaS), software as a service

* PhD advisors: Pedro García and Carlos Molina

(SaaS) and infrastructure as a service (IaaS). This allows users to deploy chosen services and client content, including client applications and data within the IBM cloud environment. At the present moment, IBM provides 18 availability zones in six global regions across the world located in the United States (Washington DC and Dallas), UK, Germany, Australia and Japan.

To perform the simulations, we have assumed PDAL library[2] and Pywren-ibm tool [4] that is an advanced extension of PyWren[3], an open source project that executes user's Python code and its dependencies as serverless actions on a serverless platform. The new features that the Pywren-ibm tool provides range from automatic data discovering, data partitioning among others. However, it is still in a development stage and it has to face many challenges before it becomes completely stable.

Particularly, the services that we have also assumed are IBM cloud functions (FaaS) and IBM cloud object storage (COS). On one hand, FaaS (Functions as a Service) is a subset of serverless computing service that allows to implement the application code in response to events without the need to know the complex details of the infrastructure, especially related to building and launching micro-services applications. On the other hand, COS is a storage service that can be managed to store unstructured data in a reliable manner, where is designed for high durability, flexibility and security. These services allow us to launch from 1 function (sequential execution) to many functions (parallel execution).

Commonly, a parallel execution in the IBM Cloud system behaves as follows: (1) the user uploads a file of a certain file together with the algorithm that processes this data from the local PC (Personal Computer) to the COS; (2) the system reads the data file from the COS; (3) the system partitions the data file in several chunks depending on the number of chunks that the user has specified; (4) the system uploads the splitted files into the COS and launches one *Map()* function per every created chunk ; (5) the system executes every function with its partial data; (6) the system waits until all the functions are completely executed; (7) the systems merges all the partial results in a single file using a *Reducer()* function; (8) finally, the user downloads the resulted file from the COS to the local PC.

3 Classification of Times

The total time needed to perform an experiment in the IBM cloud ranges from the moment that an user uploads the algorithm and its data to the moment that the selected cloud server produce the final result. We have identified several partial times involved in the total time of any experiment. These times are the following:

- 1 **PC Uploading Time (A Time)**: the time needed to upload a file from the local PC of the user to the COS on the Cloud.

- 2 Partitioning Phase Time (B Time):** this category consists of three partial times:
- a) COS Downloading Time (B1): the period of time that the partitioning function reads the data file from *COS* in order to partition it into small chunks.
 - b) Partitioning Time (B2): the period of time of splitting the file into many files.
 - c) COS Uploading Time(B3): the period of time of uploading the splitted files after the partitioning process into the *COS*.
- 3 Processing Phase Time (C Time):** this category consists of four partial times:
- a) Mapping Time(C1): the time each function takes to read its data from *COS*.
 - b) Processing Time(C2): the time of each function takes to process its data.
 - c) Obtaining Results Time(C3): the period of time needed by the reducer to get all the results from all the executed functions.
 - d) Reduction Time(C4): the time that the reducer takes to finish.

4 Analysis of Results

Our basic experiment will be performed in the IBM cloud system assuming an algorithm described in [1] that deals with a LIDAR data [5] file of 256 Megabytes (a map of several square kilometers of the Tarragona area in Spain) to remove outlier points that are classified as a noise. The same work will be done several times but varying the number of functions that will process the original LIDAR data file and partitioning it into portions of the same size. Particularly, we have performed several simulations assuming from 1 function (with a file of 256 Megabytes) to 1024 functions (each function with a partial file of 256 Kilobytes). The results obtained in these simulations can be seen in Figure 1. In this way, for each of the time categories identified in Section 3, we can identify the following behaviors:

Uploading Time (A): The Pywren-ibm partition approach only supports limited number of files types. In this case, *.txt* and *.csv* files. Therefore, we have forced to convert the *.las* file supported by LIDAR into a *.csv* file before uploading it to the *COS*. This causes an increase in the file uploading time (*A*) of approximately 3 times as the size of the converted file has been increased. As it is shown in figure1, the uploading of the data file implies a significant and similar time for all simulations except for the one that only assumes the execution of a single function. This is because with one function execution there is no need to make a partition of the file and therefore it is not needed to perform a format file conversion in the user's local PC.

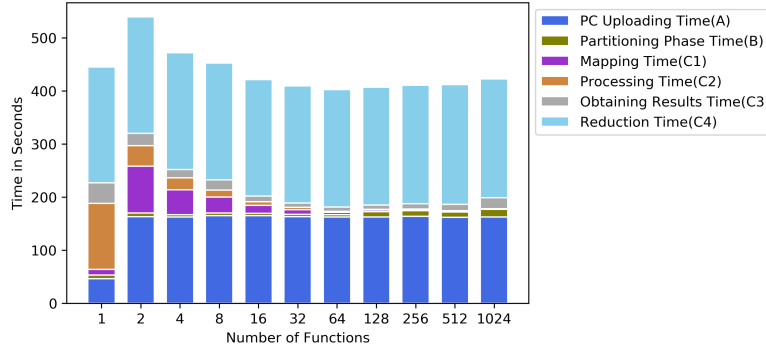


Fig. 1: Execution time depending on the number of functions

Partitioning Time (B): The Pywren-ibm partitioner takes the file data and splits it in several chunks according to the size specified by the user. Then it computes the ranges of data and assigns one range per every function. Later, each function is responsible of requesting request its data according to the assigned range. Notice that this partitioning method do no need to download and then upload the files from the COS. Nevertheless, we can observe that the time of partitioning represents a small portion of the total time involved on the execution process.

Processing Time (C): In this case, we can observe a decrease of the Mapping Time (C1) and the Processing Time (C2) as the number of functions launched are increased. This is due to the fact the size of data that each function assumes is getting smaller and therefore reading and processing data need less time. On the other hand, Obtaining Results Time (C3) is increased when number of functions is also increased. Notice that every function needs to send the result to the reducer and therefore it can be a communication overhead when the number of requests are increased. Finally, Reduction Time (C4) is quite similar in all the simulations but we can observe that together with the Uploading Time (A) are the partial time that most contributes to total time. Definitely, that means that both times are targets for improvement.

5 Conclusion and Future work

In this work we have intended to provide a first approximation of the performance potential that a Serverless Computing System can achieve. Based on this preliminary results we identify a set of aspects of improvement that well explored can improve the overall performance of the system. This further analysis will allow users and developers to understand how to take advantage of this approach. Therefore, the next steps in this research effort will be focused on analysing the following issues:

- **Type of Algorithm:** We are currently working with LIDAR data and with an algorithm that removes the noise of a map. We plan to analyze other algorithms that work with LIDAR data and even with algorithms that works with other type of data (for instance, bioinformatic or geospatial data).
- **Variability of Data:** Here, the idea is to analyse how the variability of the data affects performance when assuming the same algorithm for all of them.
- **Data Size vs Number of Functions:** To perform an experiment in a cloud system, it is required to assume a file with a certain size and partition it to be processed by another certain number of functions. We aim to study both variables at the same time (data size vs number of functions). Therefore, files from a few megabytes to a large of gigabytes will be assumed and for each of them several simulations will be carried out varying from a single function to hundreds of them.
- **Monetary Cost of Executions:** In this case, we plan to compute the monetary cost for any potential experiment with a customize configuration and find out which is the optimum trade-off between monetary cost and performance.
- **Type of Reduction:** The Pywren-ibm tool supports two options for making the reduction of the functions: a serial and a parallel approach for all *Map()* functions. We plan to analyze both approaches in detail and propose modifications to both of them in order to achieve the minimum possible reduction time.
- **IBM Cloud Servers:** the simulations performed in this work are done in the IBM cloud site located in *Washington DC*. We want to analyse in detail all available IBM sites to identify at any moment and depending of the type of the problem, the best site to perform a simulation.
- **Cloud Servers Providers:** Similar to the previous analysis, we want to extend our simulations to other cloud service providers such as Google (Cloud Functions), Microsoft (Azure Functions) or Amazon (AWS Lambda) to see how the server provider impacts in the performance efficiency.
- **Time of the Day:** We plan to make several simulations in different times and days to see if it significantly affects the moment when an execution is performed.
- **Type of Partitioning:** At the present moment, we assume the default partitioning method that the system provides. We plan to explore other approaches as making our own partitioning method with a dedicated function for this task or avoiding the physical partition of the file. That means that every function receives the full original file but each of them only processes a particular amount of data.
- **Dynamic and Transparent Framework:** based on the results of the previous analysis, we plan to build a system that eases the user from the

tasks of deciding the best cloud site at any moment, the type of partitioning, the optimal number of functions, the best time of day to run an execution, etc. In this way, based on the requirements of the user (mainly monetary cost and time to obtain the results), this new framework will try to find the optimum way to launch an execution.

Acknowledgement. This work has been funded by the Govt. of Spain under contract TIN2016-77836-C2-1-R and the Govt. of Catalonia as Consolidated Research Group 2017-SGR-688.

References

- [1] R. Bogdan Rusu, Z. Csaba Marton, N. Blodow, M. Dolha, M. Beetz. Towards 3D point cloud based object maps for household env. *Robotics and Autonomous Sys.*, 2008.
- [2] PDAL Contributors. PDAL Point Data Abstraction Library. <https://doi.org/10.5281/zenodo.2556738>, doi: 10.5281/zenodo.2556738, 2018.
- [3] E. Jonas, Q. Pu, S. Venkataraman, I. Stoica, B. Recht. Occupy the cloud: Distributed computing for the 99%. *Procs. of the 2017 Symposium on Cloud Computing*, 2017.
- [4] J. Sampé, G. Vernik, M. Sánchez-Artigas, P. García-López. Serverless data analytics in the ibm cloud. *Procs. of the 19th International Middleware Conference Industry.*, 2018.
- [5] B. Lohani, and S. Ghosh, Airborne LiDAR technology: a review of data collection and processing systems *Procs. of the National Academy of Sciences, India Section A*, 2017.

Quasi-ordinarization transform of a numerical semigroup

José Miguel Serradilla *

Department of Computer Engineering and Mathematics, Universitat Rovira i Virgili
Tarragona, Spain
josemiguel.serradilla@estudiants.urv.cat

1 Introduction

In this work, aiming to become a PhD Thesis, we are extending a partially proved conjectured for a special kind of numerical semigroups, ordinary semigroups, to an even more special kind, the quasi-ordinary semigroups. The main idea is approaching this problem paralleling the mentioned families of semigroups by using both analytical procedures and the construction of different trees and forests whose nodes are numerical semigroups.

2 Numerical semigroups

Let \mathbb{N}_0 denote the set of non-negative integers.

Definition 1. *A numerical semigroup is a subset of \mathbb{N}_0 which is closed under addition, contains 0, and its complement in \mathbb{N}_0 is finite.*

Example 1. The amount of money one can get from a cash point when the machine only withdraws notes of 20 and 50 (divided by 10):

$$S = \{0, 2, 4, 5, 6, 7, 8, \rightarrow\}$$

Example 2. In a popular hamburger shop, you can only buy packs of chicken nuggets with either 4, 5 or 9 pieces inside. What different numbers of chicken nuggets can you obtain?

$$S = \{0, 4, 5, 8, 9, 10, 12, \rightarrow\}$$

Example 3. Numerical semigroups model Weierstrass non-gaps, an approach to algebraic geometry and AG codes.

* PhD advisor: Maria Bras-Amorós

Example 4. They appear in music theory, as they are the inherent structure of the set of numbers of semitones of the intervals of each overtone of a given fundamental tone with respect to the fundamental tone, when the physical model of the harmonic series is discretized into an equal temperament.

Definition 2. Let S be a numerical semigroup.

1. The elements in $\mathbb{N}_0 \setminus S$ are called gaps.
2. The number of gaps is the genus of S . It will be denoted as g .
3. The largest gap is called the Frobenius number. It will be denoted as F .
4. The non-gap right after the Frobenius number is called the conductor. It will be denoted as c .
5. The multiplicity is its first non-zero non-gap. It will be denoted as m .
6. The generators of a numerical semigroup are those non-zero non-gaps which cannot be obtained as the sum of two smaller non-gaps.

Remark 1. Clearly, $c = F + 1$

Example 5. Let S be the semigroup seen in **Example 2**.

1. Its gaps are the elements of the set $\{1, 2, 3, 6, 7, 11\}$
2. $g(S) = 6$
3. $F(S) = 11$
4. $c(S) = 12$
5. $m(S) = 4$
6. The generators of S are the elements of the set $\{4, 5, 9\}$. We will write it this way:

$$S = \langle 4, 5, 9 \rangle$$

Definition 3. A numerical semigroup other than \mathbb{N}_0 is said to be ordinary if its gaps are all in a row.

Example 6. Let $S = \langle 3, 4, 5 \rangle$ given by its generators. The semigroup it would be $S = \{0, 3, \rightarrow\}$, which clearly is ordinary as its gaps, $\{1, 2, 3\}$, are in a row.

Definition 4. A numerical semigroup is said to be quasi-ordinary if $m = g$, that is to say, there is only one gap larger than m .

Definition 5. Let S be a semigroup with Frobenius number F .

1. The sub-Frobenius number of S is the Frobenius number of $S \cup \{F\}$.
2. The subconductor of S is the smallest nongap in its interval of nongaps immediately previous to F .

3 Ordinarization transform and the ordinarization number of a numerical semigroup

Definition 6. *The ordinarization transform of a non-ordinary semigroup S with Frobenius number F and multiplicity m is the set $S' = S \setminus \{m\} \cup \{F\}$.*

We can iterate this process until we obtain an ordinary semigroup $\{0, g + 1, g + 2, \rightarrow\}$, where g is the genus of S , iterating i times. This number is called the ordinarization number of S .

Example 7. Let $S = \langle 2, 5 \rangle = \{0, 2, 4, 5, \rightarrow\}$. We can easily see that $m = 2$ and $F = 3$. Then, $S' = \{0, 3, 4, 5, \rightarrow\}$, which is ordinary. Besides, its ordinarization number is 1.

3.1 Conjecture 1

Let $n_{g,r}$ be the number of numerical semigroups of genus g and ordinarization number r . For each genus $g \leq 49$ it has been computed in [1] $n_{g,r}$ for each ordinarization number r from 0 up to $\lceil \frac{g}{2} \rceil$. One can observe that for each ordinarization number r , the number of semigroups for this r increases with the genus or stays the same. By extending the definition of $n_{g,r}$ for $r > \lceil \frac{g}{2} \rceil$ by setting $n_{g,r} = 0$ in this case, this leads to the next conjecture:

Conjecture 1. For each genus $g \in \mathbb{N}_0$ and each ordinarization number $r \in \mathbb{N}_0$,

$$n_{g,r} \leq n_{g+1,r}$$

Remark 2. **Conjecture 1** has been partially proved in [1]

4 Quasi-ordinarization transform and the quasi-ordinarization number of a numerical semigroup

Definition 7. *The quasi-ordinarization transform of a non-ordinary semigroup S with multiplicity m , genus g and sub-frobenius number f is the set $S' = S \cup \{f\} \setminus \{m\}$.*

The quasi-ordinarization transform of a non-ordinary semigroup of genus g and conductor c can be applied subsequently and at some step we will attain the quasi-ordinary semigroup of that genus and conductor, that is, the numerical semigroup $\{0, g, g + 1, \dots, c - 2, c, c + 1, \rightarrow\}$. The number of such steps is defined to be the *quasi-ordinarization number* of S .

Example 8. Let $S = \langle 2, 11 \rangle = \{0, 2, 4, 6, 8, 10, 11, \rightarrow\}$. We can easily see that $m = 2$ and $f = 7$. Then, $S' = \{0, 4, 6, 7, 8, 10, 11, \rightarrow\}$, which is not quasi-ordinary yet. In this case, $m = 4$ and $f = 5$. Therefore, $S'' = \{0, 5, 6, 7, 8, 10, 11, \rightarrow\}$. S'' is quasi-ordinary, and its quasi-ordinarization number is 2.

Remark 3. 1. The *quasi-ordinarization* of either an ordinary or quasi-ordinary semigroup is defined to be itself.

2. In the ordinarization and quasi-ordinarization transform we replace the multiplicity by the largest and second largest gap, respectively, and we obtain numerical semigroups. In general, if we replace the multiplicity by the third largest gap, we do not obtain a numerical semigroup.

We denote by $n_{g,q}$ the set of numerical semigroups with genus g and quasi-ordinarization number q .

4.1 Conjecture 2

We can observe a behavior of $n_{g,q}$ very similar to the behavior of $n_{g,r}$ introduced in [1]. The purpose of this work is paralleling the **Conjecture 1**, that is, we conjecture that for each genus $g \in \mathbb{N}_0$ and each quasi-ordinarization number $q \in \mathbb{N}_0$,

$$n_{g,q} \leq n_{g+1,q}.$$

5 Conclusion

What has to be proved exceeds by far the length of this extended abstract. By fixing a genus g , we can define a graph whose nodes are all semigroups of such genus and whose edges connect each semigroup to its quasi-ordinarization transform, supposing it's not itself. The graph is a forest \mathcal{F}_g rooted at all ordinary and quasi-ordinary semigroups of genus g . In particular, the quasi-ordinarization transform defines, for each fixed genus and conductor, a tree rooted at the quasi-ordinary semigroup for that genus and conductor. This forest will lead us to proof **Conjecture 4.1**.

References

- [1] Maria Bras-Amorós, *The ordinarization transform of a numerical semigroup and semigroups with a large number of intervals*, Journal of Pure and Applied Algebra 216 (2012) 2507–2518.
- [2] J.C.Rosales, P.A.García-Sánchez, J.A.Jiménez Madrid, *Numerical semigroups*, in: Developments in Mathematics, vol. 20, Springer, New York, 2009.

Secure total domination in rooted product graphs

Abel Cabrera Martínez ^{*} ^{**}

Department of Computer Engineering and Mathematics, Universitat Rovira i Virgili
Tarragona, Spain
abel.cabrera@urv.cat

1 Introduction

The following approach to the protection of a graph was proposed by Cockayne et al. [5]. Suppose that one or more entities are stationed at some of the vertices of a graph G and that an entity at a vertex can deal with a problem at any vertex in its closed neighbourhood. In general, an entity could consist of an observer, a robot, a guard, a legion, and so on.

Informally, we say that a graph G is protected under a given placement of entities if there exists at least one entity available to handle a problem at any vertex. Various strategies have been considered, under each of which the graph is deemed protected. As we can expect, the minimum number of entities required for protection under each strategy is of interest.

The simplest strategies of graph protection are related with the concepts of domination and total domination of graphs. In such cases, the sets of vertices containing the entities are dominating sets, total dominating sets or their variants, respectively. Next, we expose some of these strategies. Typically, a vertex in a graph $G = (V(G), E(G))$ dominates itself and its neighbouring vertices. A subset $S \subseteq V(G)$ is said to be a *dominating set* of G if S dominates every vertex of G , while S is said to be a *double dominating set* of G if S dominates every vertex of G at least twice. A subset $S \subseteq V(G)$ is said to be a *total dominating set* of G if every vertex $v \in V(G)$ is dominated by at least one vertex in $S \setminus \{v\}$. The minimum cardinality among all dominating sets of G is the *domination number*, denoted by $\gamma(G)$. The *double domination number* and the *total domination number* of G are defined by analogy, and are denoted by $\gamma_{\times 2}(G)$ and $\gamma_t(G)$, respectively. Likewise, a set $S \subseteq V(G)$ of vertices of a graph G is a *2-dominating set* if every vertex of $V(G) \setminus S$ has at least two neighbours in S . The *2-domination number* of G is the minimum cardinality among all 2-dominating sets of G , and it is denoted by $\gamma_2(G)$.

^{*} PhD advisor: Juan Alberto Rodríguez Velázquez

^{**} Other collaborators: Alejandro Estrada Moreno (URV)

A total dominating set S is said to be a *secure total dominating set* of G if for each vertex $u \in V(G) \setminus S$, there exists a vertex $v \in S$ adjacent to u such that $(S \setminus \{v\}) \cup \{u\}$ is a total dominating set of G as well. The *secure total domination number* of G , denoted by $\gamma_{st}(G)$, is the minimum cardinality among all secure total dominating sets of G . This last concept was introduced by Benecke et al. in [1] and also studied in [2,3,4,6,7].

The problem of computing $\gamma_{st}(G)$ is NP-hard [6], even when restricted to chordal bipartite graphs, planar bipartite graphs with arbitrary large girth and maximum degree three, split graphs and graphs of separability at most two. This quotation suggests finding the secure total domination number for some special classes of graphs or obtaining tight bounds on this parameter. This is precisely the aim of this work in which we study the case of rooted product graphs.

1.1 Notation

All graphs considered in this work are finite and undirected, without loops or multiple edges. Given a vertex v of G , $N(v)$ will denote the *open neighbourhood* of v in G . The *closed neighbourhood*, denoted by $N[v]$, equals $N(v) \cup \{v\}$. Given a set $S \subseteq V(G)$, its open neighbourhood is the set $N(S) = \cup_{v \in S} N(v)$, and its closed neighbourhood is the set $N[S] = N(S) \cup S$.

We say that a vertex $v \in V(G)$ is a *universal vertex* if $N[v] = V(G)$. A *leaf* of G is a vertex of degree one. A *support vertex* of G is a vertex adjacent to a leaf, a *strong support vertex* is a support vertex which is adjacent to at least two leaves and a *strong leaf* is a leaf which is adjacent to a strong support vertex. The set of leaves, support vertices and strong leaves are denoted by $L(G)$, $S(G)$ and $L_s(G)$, respectively. If there exists a leaf $v \in L(G) \setminus L_s(G)$, then we say that v is a *weak leaf*, and the set of weak leaves is denoted by $L_w(G) = L(G) \setminus L_s(G)$.

2 Some results on the secure total domination number of rooted product graphs

In this section we present some results that allow us to analyse the secure total domination number of rooted product graphs. Firstly, we introduce the definition of this specific product graph.

Given a graph G of order n and a graph H with root vertex v , the rooted product $G \circ_v H$ is defined as the graph obtained from G and H by taking one copy of G and n copies of H and identifying the i^{th} vertex of G with the vertex v in the i^{th} copy of H for every $i \in \{1, 2, \dots, n\}$. If H or G is the empty graph, then $G \circ_v H$ is equal to G or H , respectively. In this sense, to obtain the rooted product $G \circ_v H$, hereafter we will only consider graphs G and H of orders greater than or equal to two.

Theorem 1. *For any graphs G and H with no isolated vertex and any vertex $v \in V(H)$,*

$$\gamma_{st}(G \circ_v H) \leq n(G)\gamma_{st}(H).$$

Furthermore, if $v \in V(H) \setminus S(H)$, then

$$\gamma_{st}(G \circ_v H) \leq \gamma_{st}(G) + n(G)\gamma_{st}(H - \{v\}).$$

The following result states the intervals in which the secure total domination number of a rooted product graph can be found.

Theorem 2. *Let G and H be two graphs with no isolated vertex. At least one of the following statements holds for every vertex $v \in V(H) \setminus L_w(H)$.*

- (i) $\gamma_{st}(G \circ_v H) = n(G)\gamma_{st}(H)$.
- (ii) $n(G)(\gamma_{st}(H) - 1) \leq \gamma_{st}(G \circ_v H) \leq \gamma_{st}(G) + n(G)(\gamma_{st}(H) - 1)$.
- (iii) $2\gamma_2(G) + n(G)(\gamma_{st}(H) - 2) \leq \gamma_{st}(G \circ_v H) \leq \gamma_{st}(G) + n(G)(\gamma_{st}(H) - 2)$.
- (iv) $\gamma_{\times 2}(G) + n(G)(\gamma_{st}(H) - 2) \leq \gamma_{st}(G \circ_v H) \leq \gamma_{st}(G) + n(G)(\gamma_{st}(H) - 2)$.

The following result is an immediate consequence of theorem above.

Theorem 3. *Let G and H be two graphs with no isolated vertex and $v \in V(H) \setminus L_w(H)$. If $\gamma_{st}(H - \{v\}) = \gamma_{st}(H) - 2$ and $\gamma_{st}(G) = \gamma_{\times 2}(G)$, then*

$$\gamma_{st}(G \circ_v H) = \gamma_{st}(G) + n(G)(\gamma_{st}(H) - 2).$$

We now consider some particular cases in which we impose some additional restrictions on H . We begin with the cases in which $v \in S(H) \cup L_s(H)$.

Theorem 4. *Let G and H be two graphs with no isolated vertex. The following statements hold.*

- (i) *If $v \in S(H)$, then $\gamma_{st}(G \circ_v H) = n(G)\gamma_{st}(H)$.*
- (ii) *If $v \in L_s(H)$, then $\gamma_{st}(G \circ_v H) = \gamma(G) + n(G)(\gamma_{st}(H) - 1)$.*

Finally, we analyse the secure total domination number of rooted product graph $G \circ_v H$ for the case in which the root v is a universal vertex of H .

Theorem 5. *If G is a graph with no isolated vertex, then for every graph H having a universal vertex $v \in V(H)$,*

$$\gamma_{st}(G \circ_v H) = n(G)\gamma_{st}(H).$$

The corona graph $G \odot G'$ is a rooted product graph $G \circ_v H$ where $H \cong K_1 + G'$ and v is the vertex of K_1 .

Theorem 6. *If G is a graph with no isolated vertex, then for every graph G' ,*

$$\gamma_{st}(G \odot G') = n(G)(\gamma(G') + 1).$$

Acknowledgement. This work is supported by Martí-Franquès Predoctoral Research Grant 2017PMF-PIPF-63, from Universitat Rovira i Virgili.

References

- [1] S. Benecke, E. J. Cockayne, C. M. Mynhardt. Secure total domination in graphs. *Utilitas Mathematica*, 74: 247–259, 2007.
- [2] A. Cabrera Martínez, L. P. Montejano, J. A. Rodríguez-Velázquez. On the secure total domination number of graphs. *Symmetry*, 11(9): 1165, 2019.
- [3] A. Cabrera Martínez, L. P. Montejano, J. A. Rodríguez-Velázquez. Total weak roman domination in graphs. *Symmetry*, 11(6): 831, 2019.
- [4] A. Cabrera Martínez, J. A. Rodríguez-Velázquez. Total protection of lexicographic product graphs. *Submitted*, 2019.
- [5] E. J. Cockayne, P. J. P. Grobler, W. R. Gründlingh, J. Munganga, J. H. van Vuuren. Protection of a graph. *Utilitas Mathematica*, 67: 19–32, 2005.
- [6] O. Duginov. Secure total domination in graphs: bounds and complexity. *Discrete Applied Mathematics*, 222: 97–108, 2017.
- [7] W. F. Klostermeyer, C. M. Mynhardt. Secure domination and secure total domination in graphs. *Discussiones Mathematicae Graph Theory*, 28 (2): 267–284, 2008.

Using The Feedback of Dynamic Active-Pixel Vision Sensor (Davis) to Prevent Slip in Real Time

Armin Masoumian *

Department of Computer Engineering and Mathematics, Universitat Rovira i Virgili
Tarragona, Spain

armin.masoumian@estudiants.urv.cat

1 Abstract

The objective of this paper is to describe an approach to detect the slip and contact force in real-time feedback. In this novel approach DAVIS camera used as a vision tactile sensor due to its fast process speed and high resolution. Two hundred experiments were performed on four objects with different shape, size, weight and material to compare the accuracy and respond of the Baxter robot grippers to avoid slipping. The advanced approach is validated by using a force-sensitive resistor (FSR402). The events captured with DAVIS camera are processed with specific algorithms to provide feedback to the Baxter robot aiding it to detect the slip.

Keywords: vision sensor; tactile sensor; baxter robot; real-time feedback; vision-based slip detection

2 Introduction

Though the sensors are good in detecting slip of the objects they will not be able to apply the minimum force required so that the object does not deform. This will be destructive in the case of fragile objects. The slip is detected only when a shear force is produced and the object slips away. The idea of using a camera to detect the slip will overcome these disadvantages. The input from the camera can also be used in conjunction with deep learning algorithms to benefit from incipient slip detection. The Baxter robot is an industrial robot built by rethink robotics [2]. It has two arms with an animated face. Since the robot is mainly used in assembly and manufacturing lines, a safety feature has been built into the robot which is capable of sensing humans near-by and restricting its motion. Thus it eliminates the need to be in a caged working environment unlike other robots. The Baxter achieves this by having multiple sensors in its hand and arms, while the motors actuate the joints through springs. The springs provide a cushioning effect and make it less hazardous as

* PhD advisor: Domenec Puig Valls

it is able to reduce the force before collision. The Baxter robot is capable of learning complicated movements in a unique way. The robot's hand can be moved physically by a person in the desired way and the robot is capable of memorizing the motion and replicating it. There is a single mounted camera on Baxter last joint which can be used for teaching Baxter to do tasks [1]. For this project, a transparent gripper needs to get the events of the contacted area, therefore, a new gripper designed with acrylic and transparent silicone. The DAVIS camera is a unique type of camera, the method in which it acquires inputs sets it apart from the traditional cameras. It is inspired by the function of the human eye and tries to mimic it. Knowing how this approach benefits functioning for eyes, researchers are developing machine-vision frameworks in which every pixel modifies its own inspecting because of changes in the measure of incident light it gets. This method of capturing data is called level-crossing sampling. Each pixel is attached to a level-crossing detector and a separate exposure-measurement circuit. The amplitudes of each pixel are measured and checked in a reference to a previously measured threshold value or compared with the previous signal, if below the previous signal the new level is recorded and used as reference. In addition, the DAVIS camera can be used to detect the deformation of the object during grasping by the Baxter grippers [4]. This camera has a high-speed computer vision because it works mostly with event-based, which has low latency, high temporal resolution, and very high dynamic range [3].

3 Experimental Setup

Since the event camera only gets pixels that change they have advantages over traditional cameras. They do not process redundant information (only captures pixels that change) hence they save a lot of memory, do not waste computational energy on redundant pixels, do not suffer from latency as they do not have to wait for unnecessary frames and has a very high temporal resolution, very high dynamic range and low power and bandwidth requirements. DAVIS240C camera has been used for detecting the slip of the object in a millisecond and then sending the feedback of the DAVIS camera to the gripper of the Baxter robot. DAVIS camera has been mounted on behind the grippers with a specific angle, which based on the brightness of the light, will detect the touching area of the object and gripper. Therefore, gripper must be transparent so the camera can see the object through the gripper, and gripper must be made of soft tissue materials so that by deformation of the gripper camera will detect whether or not slip is happen. Transparency and thickness of the silicone grippers are quite important in this task because much transparency can cause a lot of noise in the background of the object. If the thickness of the silicone is big, the contact area will not be clear in the DAVIS camera and if the thickness is too thin, then it will not capture the deformation the silicone and object can slip easily through the grippers. To prove that force is changing in Baxter grippers, force sensitive resistor has been set and coded in Raspberry PI 2B to validate the value of the force. The FSR402 is a Force Sensitive Resistor which is a robust polymer thick film (PTF) device which shows a decrease in resistance by increasing the force applied to the sensor surface. FSR has been developed to use in electronic devices, which needs to be controlled by human touch such as automotive electronics, medical systems. FSR402 will show the force in a range of 0 to 1024, although this number can be changed based on a resistor that has been set for this sensor. This resistance depends on the

amount of pressure that will be applied on the sensor which is more force will cost less resistance and less force will make high resistance and if there is no pressure on the sensing area, the resistance will be bigger than 1M. This sensor can sense applied force anywhere in the range of 100g-10kg. Robot Operation System, known as ROS, is an open-source mixture of middle ware and operating systems for robots. This meta-operating system provides the services that expect from a robot operating system such as hardware abstraction, low-level device control, implementation of commonly used functionality, message passing between processes, and package management. One of the most advantages of ROS is that it can provide a huge amount of tools for configuring the setup for the robot, start programming, testing and analyzing the results debugging the problems and many more possibilities. In addition, ROS has the availability to use many libraries that implement useful robot functionality, with a focus on mobility, manipulation, and perception.

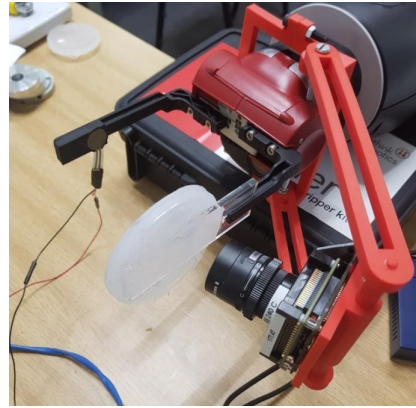


Fig. 1: Assembly Setup on Baxter Gripper

Analogue image processing will analyze and manipulate the hard copy of the image. However, digital image processing will analyze and manipulate the image in a computer with image processing software. The noise filter is used to filter out noises in the background of the frame that is focused upon. The noise filter works by using the concept of hot pixels. Hot pixels can be considered as an abnormal behavior of pixels. An object with a specific size would produce at least more than two or three pixels depending upon the distance. If the object is too far away it is entirely a different story. Any change of an object very far away would be represented as a single pixel. For learning which pixels are hot pixels or not, the two parameters, which is explained above, is taken as an input form the user. The time period in microseconds to accumulate events for learning hot pixels and the number of events needed in a learning time period to consider a pixel hot. The contact area is the area of the object that is touching the silicone in the gripper. Finding out the contact area helps to determine the slip of the object efficiently. The contact area is determined by capturing the events from the camera when the gripper is closing in on the objects. Objects coming in contact with silicone will produce negative polarity events at the point of contact because they block the incoming light to the camera. Based on the results from image processing, if the camera detects the slip happening, then, the

gripper position will be reduced to prevent slip. This was the feedback between the camera and the Baxter robot and is done with socket programming. However, the important part is gripper must know how much needed to be closed or opened to stop slipping. Because if the gripper position is being reduced too much, then it will deform or even break the object. For finding the best values for the gripper position in each period, the PID controller has been programmed for this task, which will be explained in the next section.

4 PID Control

The PID controller is employed in this research as a means of feedback and to control the force of the grippers. The gripper position parameter is used as a means of controlling the force. The PID controller works by receiving an error, which is a deviation from a specified set point and adjusts the control outputs in order to drive the error to zero. The three values namely, proportional, integral and derivative determine how quickly and accurately the error is driven to zero. The error in this setup would be the number of positive polarity events captured in the contact area while the program is running. Also, the error has to be updated after each timeframe, called the sample time. The sample time chosen for this setup is one millisecond.

5 Results

For each object, two parameters of the gripper position and force sensor value have been discussed. The first graph represents the gripper positions of the gripper and the second graph represents the force sensor values. Based on the 200 experiments, cube shape objects have more accurate results than spherical objects because the contact area is bigger. Because of the vibration of robot arms, there are a little fluctuation in force sensor values.

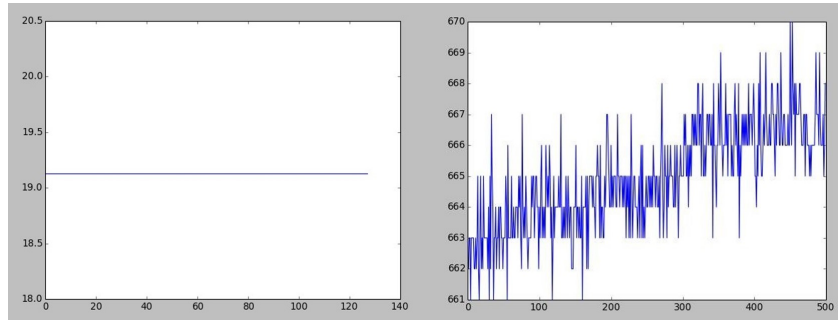


Fig. 2: Gripper position and Force sensor values for plastic box 110 gr

Sometimes there is a difference between number of force values and gripper position values, because the times, which slip is not happening, the results will be same and gripper will not count the values, but force sensor will capture all values till one cycle period time will be down, which in this experiment all cycle were 20 seconds.

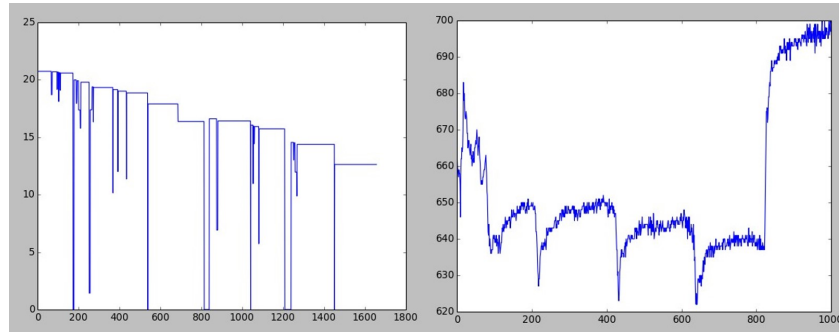


Fig. 3: Gripper position and Force sensor values for plastic box 1360 gr

6 Conclusion

In this paper, a novel method approach was proposed to detect the slip and contact force in real-time feedback. DAVIS camera was used as a vision tactile sensor for fast process and high resolution. Socket programming was also used to get close-loop in real-time feedback. The advanced approach is validated by using a force-sensitive resistor (FSR402). The events captured with the DAVIS camera were processed with algorithms to provide feedback to the Baxter robot aiding it to detect slip. All devices are synchronized to avoid any delays. PID controller was used for stabilizing the system to get more accurate results.

References

- [1] Huang, Yanjiang and Zhang, Xianmin and Chen, Xunman and Ota, Jun. Vision-guided peg-in-hole assembly by Baxter robot , *Advances in Mechanical Engineering*, 9, 2017, SAGE Publications Sage UK: London, England
- [2] Inzunza, Sergio and Juárez-Ramírez, Reyes and Jiménez, Samantha. Api documentation, *World Conference on Information Systems and Technologies*, 229–239, 2018, Springer
- [3] Mueggler, Elias and Rebecq, Henri and Gallego, Guillermo and Delbruck, Tobi and Scaramuzza, Davide. The event-camera dataset and simulator: Event-based data for pose estimation, visual odometry, and SLAM. *The International Journal of Robotics Research*, 36, 142–149, 2017, SAGE Publications Sage UK: London, England
- [4] Zhao, Kai and Li, Xueyong and Lu, Changhou and Lu, Guoliang and Wang, Yonghui. Video-based slip sensor for multidimensional information detecting in deformable object grasp. *Robotics and Autonomous Systems*, 91, 71–82, 2017, Elsevier

A Human Assisted Model for Engineering Drawing Validation

Elena Rica *

Department of Computer Engineering and Mathematics, Universitat Rovira i Virgili
Tarragona, Spain
mariaelena.rica@urv.cat

1 Introduction

Piping and Instrumentation Diagrams (P&IDs) are frequently used for the representation of the structure and components in Oil & Gas industry. Last years, there has been an increased effort to migrate these printed engineering drawings towards a digital environment throw collaborations between industrial partners and the research community². This has been tested by numerous authors [3],[10],[6],[7],[8],[4], and some methods have appeared which automatically generate a CAD document given the paper sheets. Due to the complexity of this process and the need of being a zero error process, this final CAD document is always verified by an engineer.

This paper is an abstract of article [9] in which we present a method that reduces the required engineer working time throw the automatic detection of possible incorrectly identified components in the generated CAD model.

2 CAD model generation and automatic P&ID validation

Figure 1 shows the general schema of the method we propose in [9]. We explain below the main characteristics:

Given a *Paper P&ID*, the generation of an *Automatic CAD* model representing its information requires two main steps. Firstly, the digitisation step consists on detect and localise the main shapes of the P&ID and create a netlist containing the positions of each element. Secondly, the contextualisation step makes sense out of the previously digitised data describing the connections and relations between the components.

After the Digitisation & Contextualization step, the *Automatic CAD* needs to be validated to guarantee the correctness of the obtained components and

* Susana Álvarez, Francesc Serratosa

² <https://cfmgcomputing.blogspot.com/2018/06/rgu-and-dnv-gl-join-forces-to-create.html>

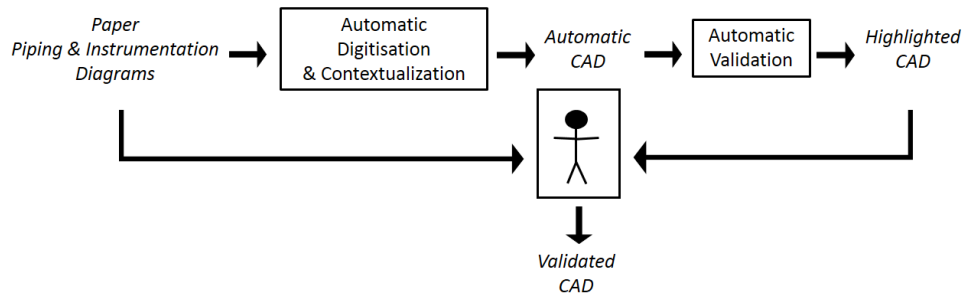


Fig. 1: Main schema of the method presented in [9] to assist the human validation of P&IDs.

structures. Then the Automatic Validation module detects the possibly incorrectly identified components in the *Automatic CAD*.

This module is implemented defining an attributed graph representing the P&ID. Attributed graphs are commonly used in pattern recognition processes and they are a powerful tool (see reviews [1,11,5,2]). In our situation, the nodes represent the components and the edges represent the pipelines connecting them. Moreover, nodes have only one attribute which is the component identity and edges are undirected and unattributed. The graph is embedded in an Euclidean space and then a neural network is applied. Then, a verification module analyses the results and proposes the possible incorrectly identified components in a *Highlighted CAD*. The human expert just need to validate these elements and the property of zero error process is maintained with a considerable reduction of work.

3 Conclusions and future work

We have developed a method to reduce the effort in the human validation of *Automatic CAD* models representing P&IDs. The experimental results show that we achieve a reduction of approximately the 40% of human effort keeping a zero-error process.

As a future work, we want to analyse different configurations of the defined neural network and analyse if a deep neural network could be used. We also want to apply the method to P&IDs of other industries and we believe our method could really decrease the economical and temporal cost of this task.

Acknowledgement. This research is supported by Spanish projects TIN2016-77836-C2-1-R and DPI2016-78957-R, by the Data Lab and the Oil & Gas Scottish Innovation Centres, and by Det Norske Veritas Germanischer Lloyd (DNV GL).

References

- [1] Donatello Conte et al. "Thirty years of graph matching in pattern recognition". In: *International journal of pattern recognition and artificial intelligence*, 18.03 (2004), pp.265–298.
- [2] Pasquale Foggia, Gennaro Percannella, and Mario Vento. "Graph matching and learning in pattern recognition in the last 10 years". In: *International Journal of Pattern Recognition and Artificial Intelligence* 28.01(2014), p. 1450001.
- [3] C. Howie et al. "Computer Interpretation of Process and Instrumentation Drawings". In: *Advances in Engineering Software* 29.7-9 (1998), pp. 563–570. ISSN: 09659978. DOI:10.1016/S0965-9978(98)00022-2.
- [4] Sung-O Kang, Eul-Bun Lee, and Hum-Kyung Baek. "A digitization and conversion tool for imaged drawings to intelligent piping and instrumentation diagrams (P&ID)". In: *Energies* 12.2593 (2019), pp. 1–26. DOI:10.3390/en12132593
- [5] Lorenzo Livi and Antonello Rizzi. "The graph matching problem". In: *Pattern Analysis and Applications*16.3 (2013), pp. 253–283
- [6] Carlos Francisco Moreno-García, Eyad Elyan and Chrisina Jayne. "Heuristics-Based Detection to Improve Text / Graphics Segmentation in Complex Engineering Drawings". In: *Engineering Applications of Neural Networks*. Vol. CCIS 744.2017, pp. 87–98
- [7] Rohit Rahul et al. "Automatic Information Extraction from Piping and Instrumentation Diagrams". In: *International Conference on Pattern Recognition Applications and Methods (ICPRAM)*. 2019, pp. 163–172. DOI: 10.5220/0007376401630172. arXiv: 1901.11383. URL:<http://arxiv.org/abs/1901.11383>
- [8] Miia Rantala et al. "Applying graph matching techniques to enhance use of plant design information". In: *Computers in Industry* 107(2019), pp. 81–98. ISSN: 01663615. DOI:10.1016/j.compind.2019.01.005. URL:<https://doi.org/10.1016/j.compind.2019.01.005>.
- [9] Elena Rica et al. "Reducing human effort in engineering drawing validation" In: *Computers in Industry* 117 (2020), p. 103198
- [10] Wei Chian Tan, I. Ming Chen, and Hoon Kiang Tan. "Automated identification of components in raster piping and instrumentation diagram with minimal pre-processing". In: *IEEE International Conference on Automation Science and Engineering*, November (2016), pp. 1301–1306. ISSN: 21618089. DOI:10.1109/COASE.2016.7743558.
- [11] Mario Vento. "A long trip in the charming world of graphs for pattern recognition". In: *Pattern Recognition* 48.2 (2015), pp. 291–301

The deployment of a decision support system for the diagnosis of Diabetic Retinopathy into a Catalan medical center

Emran Saleh, Najlaa Maarooof, Mohammed Jabreel *

Department of Computer Engineering and Mathematics, Universitat Rovira i Virgili Tarragona, Spain

1 Introduction

Diabetes Mellitus (DMs) is a chronic disease that affects 382 million patients worldwide (2013 data) and is predicted to increase to as many as 592 million adults by 2035. In Spain, we predict an incidence of over 3 million DM sufferers by 2030 [3]. People suffering from DM may have different derived health complications, in particular, we focus on studying the Diabetic Retinopathy (DR) disease. Diabetic Retinopathy causes lesions in the eye, in particular, in the retina. If they are not detected and treated in due time, it can cause blindness. DR is one of the significant causes of blindness in young adults around the world [1].

A screening test of the eye fundus by means of images obtained with a non-mydratic fundus camera can reveal the presence of lesions in the eye. In Catalonia (as well as Spain and many European countries), annual screening is recommended for diabetic patients. However, this treatment is costly and not feasible. Due to a large number of patients, at the moment, Catalan centers are only able to screen each patient on average every 2.5 years. Given the incidence of the disease is about 10%, most of the tests are unnecessary. Family doctors, who are in charge of continuous monitoring of diabetic people, are not experts in the diagnosis of DR. For this reason, they are not able to decide not performing a screening analysis on a particular patient. Not performing proper filtering causes an excessive increase in the cost of screening. Moreover, patients attend unnecessary tests, with a loss of time for the patients as well as for the experts that must analyze thousands of eye images collected [2].

In the last years, we have been working on the development of an intelligent decision support system that estimates the risk of developing DR using the data available in the Electronic Health Care record of diabetic patients. Depending on the risk level, the system recommends the most appropriate time for the next visit.

* PhD advisor: Aida Valls, Antonio Moreno, Domènec Puig, Pere Romero

In a study of the data available in EHR, the most significant risk factors were identified [4]. They correspond both to physical conditions (e.g. age or sex), to substances detected in blood or urine analysis (e.g. microalbuminuria) and to the variables related to the patients' treatment (e.g. control of arterial hypertension or ingestion of oral anti-diabetic medication). Finally, nine factors were selected.

The goal is that family physicians have a tool integrated with their usual software at the hospital that can be executed in order to calculate the degree of DR risk.

2 A decision support system based on fuzzy rules

This clinical decision support system consists of a set of fuzzy rules. In particular, we have a model that is a Fuzzy Random Forest, consisting of a set of 100 trees.

Machine learning algorithms are used to construct the fuzzy rules of each of the trees. In particular, we use a modified version of the Yuan&Shaw algorithm to minimize a measure of classification ambiguity based on fuzzy sets. The inference method applied to the ruleset is the Mamdani procedure combined with an aggregation operator based on Choquet integral [5]. The classification model build achieves an accuracy of 80%, with sensitivity of 81.3% and specificity of 79.7%.

3 Retiprogram at Hospital Universitari Sant Joan de Reus

Hospital Universitari Sant Joan de Reus (HUSJR) is the leading health center located in Reus (Tarragona province). This hospital serves an area of Catalonia with a population of 247174 inhabitants. The total number of diabetic patients (with type-2 DM) screened yearly has increased from 5000 to 5500 in the last 10 years, from a total of 15811 T2DM patients.

In cooperation with the computer engineers working at HUSJR, the Retiprogram is now included in the toolset of the desktop software of the doctors. Retiprogram also works as a web service, and it has been installed in a server of the hospital. A graphical interface has been developed following the rest of the software of the hospital, which helps doctors to be familiar with it and efficiently work with this new system. The frame is as simple as possible, having the input data in the left of the window and the output data at the right, as shown in Figure 1.

Most of the 9 input values are automatically retrieved from the EHR that is stored in the hospital database. If their values are missing or must be updated, the doctor introduces the new values, and the system performs the calculation. This tool shows if there is a risk or not and indicates the degree of confidence in the answer.

Fig. 1: Retiprogram at HUSJR.

As the system is not completely perfect in its predictions, the doctor must confirm or not the answer obtained. For this reason, the user can introduce comments in order to justify the decision made, especially in case of not following the recommendation given by the system.

4 Future Work

We are collecting now the feedback from the doctors in the use of the Retiprogram system. After a period of test, we will analyze the performance of the system and the comments given by the doctors in the cases where the model gives an unreasonable answer. We are also working on the explainability of the output given by the classification system, which will show to the doctor, which are the risk factors that should be corrected.

Acknowledgement. The 3 authors have been supported by pre-doctoral grants (one FI grant from Generalitat de Catalunya & two with PMF-PIPF grants from URV). The work is financed by Instituto de Investigaciones Carlos III (IISCI), Spain, nos. FI12/01535, June 2012, and FI15/01150 July 15. FEDER funds and URV grants numbers: 2015PFR-URV- B2-60, 2016PFR-URV-B2-60.

References

- [1] Pedro Romero-Aroca, Sofia De La Riva-Fernandez, Aida Valls-Mateu, Ramon Sagarra-Alamo, Antonio Moreno-Ribas, and Nuria Soler. Changes observed in diabetic retinopathy: eight-year follow-up of a spanish population. *British Journal of Ophthalmology*, 100(10):1366–1371, 2016.
- [2] Pedro Romero-Aroca, Sofia de la Riva-Fernandez, Aida Valls-Mateu, Ramon Sagarra-Alamo, Antonio Moreno-Ribas, Nuria Soler, and Domenec Puig. Cost of diabetic retinopathy and macular oedema in a population, an eight year follow up. *BMC ophthalmology*, 16(1):136, 2016.
- [3] Pedro Romero-Aroca, Raul Navarro-Gil, Aida Valls-Mateu, Ramon Sagarra-Alamo, Antonio Moreno-Ribas, and Nuria Soler. Differences in incidence of diabetic retinopathy between type 1 and 2 diabetes mellitus: a nine-year follow-up study. *British Journal of Ophthalmology*, 101(10):1346–1351, 2017.
- [4] Pedro Romero-Aroca, Aida Valls, Antonio Moreno, Ramon Sagarra-Alamo, Josep Basora-Gallisa, Emran Saleh, Marc Baget-Bernaldiz, and Domenec Puig. A clinical decision support system for diabetic retinopathy screening: creating a clinical support application. *Telemedicine and e-Health*, 25(1):31–40, 2019.
- [5] Emran Saleh, Aida Valls, Antonio Moreno, Pedro Romero-Aroca, Humberto Bustince, and Vicenc Torra. A hierarchically \perp -decomposable fuzzy measure-based approach for fuzzy rules aggregation. *International Journal of Uncertainty, Fuzziness and Knowledge-Based Systems*, 27(Suppl. 1):59–76, 2019.

Pre-service teachers' efficacy beliefs and attitude towards mathematics

Jaime Segarra Escandon *

Department of Computer Engineering and Mathematics, Universitat Rovira i Virgili
Tarragona, Spain
jaimerodrigo.segarra@urv.cat

1 Introduction

Several researchers consider that students' attitude towards mathematics and teachers' efficacy are an important factor in high-quality mathematics, since it is related to students' academic performance (e.g., [1], [2], [3]).

According to some researchers, a teacher must have positive attitudes and beliefs towards mathematics in order to achieve a successful teaching activity (e.g., [4]). Specifically, these researchers mentioned that the attitudes and beliefs of trainee teachers would influence their teaching in the future and also the attitudes and beliefs of their students.

The following research works study the teachers' efficacy beliefs and attitude towards mathematics. In [5], they studied the relationship between the mathematical anxiety of elementary school teachers, math teaching practices, and students' performance in mathematics. They showed that low-level beliefs in self-efficacy to teach math could cause mathematical anxiety, which, at the same time, can negatively influence student performance. In addition, they found a positive relationship between math anxiety and anxiety about teaching mathematics. Moreover, they found that the increase in student performance in mathematics was related to lower levels of anxiety from teaching mathematics, but was not related to general anxiety about mathematics.

More recently, in [6], they investigated the characteristics of primary school teachers, comparing their beliefs of self-efficacy in teaching mathematics. The author stated that teachers with a greater belief in self-efficacy show a higher level of effort and persistence with students, being more open to new ideas and new methods. In addition, these teachers believe in students' academic achievements and take responsibility for student success.

Besides, in [7], they examined the relationships between the efficacy of primary math teachers with the self-efficacy and mathematical performance of their students. Their results showed that math teachers' beliefs of efficacy have

* PhD advisor: Carme Julià

a significant influence on the self-efficacy and performance of their students in mathematics.

Taking into account these previous works, the objective of this research is to study the relationship between the teachers' efficacy beliefs and the attitude towards mathematics of pre-service teachers.

2 Method

The participants in this study are the third-year students of the Bachelor Degree in Primary Education at University Rovira i Virgili who attended math class the second week in the 2019-2020 academic year. Specifically, the sample of this study corresponds to 56 students out of the 95 enrolled in the third year of the Degree of Primary Education (59% of the total population), 28% of the sample were men, while 72% were women.

Two instruments were used in this research: 1) the Mathematics Teaching Efficacy Belief Instrument (MTEBI) for pre-service teachers [8], and 2) the Attitude towards Mathematics Scale (AMS) for pre-service teachers [9]. The MTEBI consists of 21 items and it provides information on its two subscales, teaching self-efficacy (PMTE) and Mathematics Teaching Outcome Expectancy (MTOE). The AMS consists of 25 items and it has five subscales (pleasure, anxiety, usefulness, motivation and confidence).

In order to determine the reliability of the obtained results, internal consistency was analyzed. It is important to indicate Cronbach's alpha for attitude towards mathematics is excellent ($\alpha = 0.93$) and for teachers' efficacy beliefs it is acceptable ($\alpha = 0.75$).

3 Results

This research explores the relationship between mathematics teachers' efficacy beliefs and attitude towards mathematics of primary pre-service teachers. Specifically, two research questions are considered in this study: 1. Is there a relationship between the mathematics teachers' efficacy beliefs of pre-service teachers and their attitude towards mathematics? 2. Are there differences between the mean the MTEBI and AMS?

Question 1, Pearson's correlation coefficient between the teachers' efficacy beliefs and attitude towards mathematics is ($\rho=0.54, p<0.01$). This result indicates that there is a significant moderate correlation between beliefs and attitude.

For a better interpretation of the correlation of the data, the scatter plot between the teachers' efficacy beliefs and attitude towards mathematics is presented. Figure 1 shows that there is a direct linear relationship between the beliefs and the attitude of pre-service teachers with a stochastic dependence.

The straight line (red line) indicates the trend line. Besides, the lowest line (blue line) indicates the local regression, it is an adjustment of data curves by smoothing.

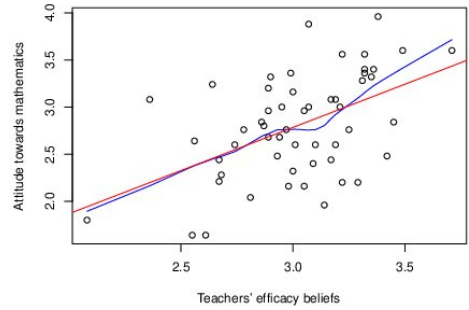


Fig. 1: Scatter plot between beliefs and attitude

Question 2, Figure 2 shows the mean of the values that each pre-service teacher gives to the teachers' efficacy beliefs and attitude towards mathematics. It can be seen that the lowest values are obtained in attitude towards mathematics.

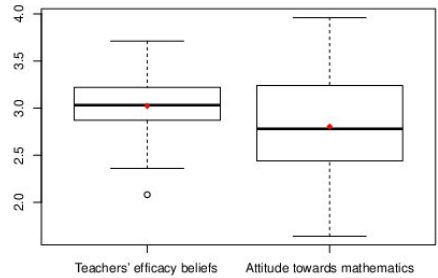


Fig. 2: Individual pre-teacher average scores given to the beliefs and attitude

Notice that the mean of the beliefs is 3.01 and standard deviation is 0.27, while the mean of the attitude is 2.80 and standard deviation is 0.68. Besides, the range of values of the attitude is clearly wider than the ones of the beliefs.

Additionally, a t-test was performed to compare the means obtained in each test. Specifically, a two-tailed test was administrated, setting $\alpha = 0.05$ as a

significance level (5%). The value of p is ($p < 0.001$), the difference between the obtained means is statistically significant beliefs and attitude.

4 Conclusions

The purpose of this research was to study relationship between mathematics teachers' efficacy beliefs and attitude towards mathematics. To carry out the research, two independent instruments were used: the MTEBI, to measure the teachers' efficacy beliefs and the AMS, to measure the attitude towards mathematics. Specifically, the study showed that the teachers' efficacy beliefs and the attitude towards mathematics have a significant moderate correlation. Additionally, the value of p indicates that the teachers' efficacy beliefs has the highest mean with respect attitude towards mathematics. The results indicate that we have to apply methodological strategies that help improve the attitude of pre-service teachers.

References

- [1] A. Bandura. Social foundations of thought and action: A social cognitive theory. *Englewood Cliffs, NJ: Prentice Hall.*, 1986.
- [2] B. Zimmerman. Self-efficacy: An essential motive to learn. *Contemporary educational psychology*, 25 (1): 82–91, 2010.
- [3] S. Recber, M. Isiksal, Y. Koç. Investigating self-efficacy, anxiety, attitudes and mathematics achievement regarding gender and school type. *Annals of Psychology*, 34 (1): 41–51, 2018.
- [4] S. Shulman. Those who understand: Knowledge growth in teaching. *Educational Researcher*, 15 (2): 4–14, 1986.
- [5] K. Hadley, J. Dorward. The Relationship among Elementary Teachers' Mathematics Anxiety, Mathematics Instructional Practices, and Student Mathematics Achievement. *Journal of Curriculum and Instruction*, 5 (2): 27–44, 2011.
- [6] O. Nurlu. Investigation of Teachers' Mathematics Teaching Self-efficacy. *International Electronic Journal of Elementary Education*, 8 (1): 21–40, 2015.
- [7] Y. Chang. Examining Relationships among Elementary Mathematics Teachers' Efficacy and Their Students' Mathematics Self-efficacy and Achievement. *Eurasia Journal of Mathematics, Science and Technology Education*, 11 (6): 1307–1320, 2015.
- [8] L. Enochs, P. Smith, D. Huinker. Establishing factorial validity of the mathematics teaching efficacy beliefs instrument. *School Science and Mathematics*, 100 (4): 194–202, 2000.
- [9] E. Auzmendi. Attitudes towards mathematics-statistics in middle and university education. *Características y medición. Ed mensajero. España*, 1992.

Protecting Consumer Privacy in Smart Metering by Randomized Response

Bastian Stölb *

Department of Computer Engineering and Mathematics, Universitat Rovira i Virgili
Tarragona, Catalonia

bastian.stoelb@estudiants.urv.cat

1 Introduction

By the end of 2018, roughly 44 percent of European households were equipped with a smart meter (SM). According to [3], by the year 2023 the distribution will be around 71 percent, which means that over 200 million homes in Europe will be equipped with smart meters.

With SMs the power usage can be observed in real time by the energy providers, thus allowing as much electricity as necessary to be produced in a specific time. However, this increase of efficiency comes at the cost of privacy.

2 Non-Cryptographic Smart Meter Privacy

The communication of smart meters with utility companies takes place over a public network (the Internet) and is regarded as unsafe unless appropriate countermeasures are taken. That is why a lot of work in this area has been performed and is still ongoing on protecting privacy. Most researchers focus on cryptographic solutions, mainly Partially Homomorphic Encryption (PHE) and Fully Homomorphic Encryption (FHE). Although cryptographic methods are appealing, one should consider the limited computational capacity of a smart meter. With this in mind, non-cryptographic solutions seem worth exploring.

2.1 Privacy models

Non-cryptographic solutions are normally oriented to satisfying a privacy model, that is, a privacy condition. As stated by Domingo-Ferrer and Soria-Comas in [1], there are four major privacy models: Randomized Response, k -anonymity, Differential Privacy and Permutation Paradigm.

* PhD advisors: Josep Domingo-Ferrer and David Sánchez

For the sake of brevity, only Randomized Response is illuminated here. Randomized Response (RR) was invented by Warner in 1965 [4] and views privacy as deniability. RR allows obtaining answers to sensitive questions (e.g. did you take drugs?) while assuring the respondent’s privacy. The respondent is allowed to randomize her answer according to some prescribed probability matrix before reporting it. Thus, she can deny that the reported answer is her true answer, but at the same time the interviewer can use his knowledge of the probability matrix to estimate the true distribution of the answers of a set of respondents from the distribution of their reported answers.

2.2 Aggregation and smart meters

Aggregation is a useful principle to achieve privacy. It is also instrumental to reduce computation and communication costs, which is very welcome in smart meters because they have constrained resources. We summarize the overview on aggregation in smart meters given by Erkin and Tsudik in [2]:

- *Spatial aggregation.* The smart meters are (geographically) clustered.
- *Temporal aggregation.* Fine-grained data is summed up by the smart meter.
- *Spatio-temporal aggregation.* Hybrid setting – a combination of both.

3 Our Proposed Scheme

3.1 Goals

We propose a non-cryptographic solution that offers the following features:

- privacy;
- simplicity (lightweight, no need for a TTP);
- support for individual readings (without aggregation);
- low computational overhead;
- low communication overhead;
- integrity;
- high accuracy.

We demonstrate our approach with real data (from the London Data Store²) and using a realistic smart meter architecture (with respect to scalability).

3.2 Rationale

The diagram in Figure 1 compares cryptographic and non-cryptographic solutions. Our aim is to develop a scheme based on RR that can handle individual readings and maintain privacy at the same time.

² <https://data.london.gov.uk/dataset/smartmeter-energy-use-data-in-london-households>

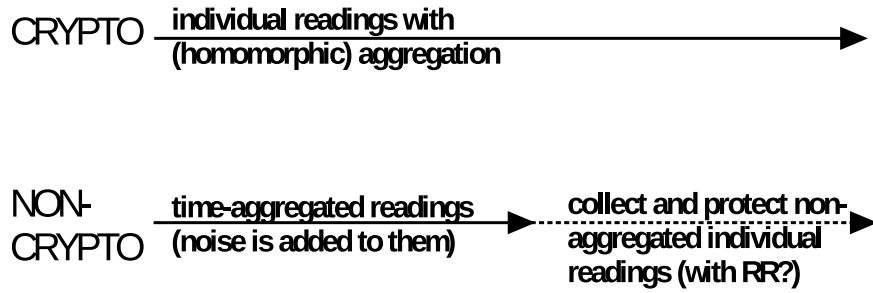


Fig. 1: Cryptographic vs. non-cryptographic solutions

4 Experimental Results

4.1 Smart meter data set

As stated above, we have used real data from the London Data Store³. 5567 households were selected as a balanced sample of London’s society. Data sets were then released with the energy consumption measured every half hour, a unique household identifier and a time-stamp. For this paper the data set UKPN-LCL-smartmeter-sample.csv was used.

4.2 Creating the RR matrix

Let us denote by X the attribute containing the answer to a sensitive question. If X can take r possible values, then the randomized response Y reported by the respondent instead of X follows an $r \times r$ matrix of probabilities

$$\mathbf{P} = \begin{pmatrix} p_{11} & \cdots & p_{1r} \\ \vdots & \vdots & \vdots \\ p_{r1} & \cdots & p_{rr} \end{pmatrix} \tag{1}$$

where $p_{uv} = Pr(Y = v|X = u)$, for $u, v \in 1, \dots, r$ denotes the probability that the randomized response is v when the respondent’s true attribute value is u . We have constructed RR probability matrices with $p = 0.4$, $p = 0.6$ and $p = 0.8$ in the main diagonal. We have filled the off-diagonal probabilities by using three different attenuation formulae A, B and C on p . In total we have 9 different probability matrices, corresponding to each value of p combined with each attenuation formula. Attenuations are as follows:

- *Attenuation formula A.* Populate the matrix with p in the main diagonal. For the super-diagonal and the sub-diagonal divide p by 2. For the super-super-diagonal and the sub-sub-diagonal divide p by 4, and so on. Finally, rescale the probabilities in each row of the matrix for them to sum to 1.

³ <https://data.london.gov.uk/dataset/smartmeter-energy-use-data-in-london-households>

- *Attenuation formula B.* Populate the matrix with p in the main diagonal. For the super-diagonal and the sub-diagonal divide p by 1 plus the distance to the diagonal. Do the same for the super-super-diagonal and the sub-sub-diagonal, and so on. Finally, rescale the probabilities in each row of the matrix for them to sum to 1.
- *Attenuation formula C.* Populate the matrix with p in the main diagonal. For the super-diagonal and the sub-diagonal raise p to the power of 1 plus the distance to the diagonal. Do the same for the super-super-diagonal and the sub-sub-diagonal, and so on. Finally, rescale the probabilities in each row of the matrix for them to sum to 1.

4.3 Analysis

Our analysis consists in comparing the distributions. To transform continuous consumption data into categorical data amenable to randomization, we have split the range of consumption into 16 intervals. The diagram in figure 2 present results corresponding to the average of 100 runs for matrix A. The abscissa in the diagram represents the intervals, and the ordinate the relative frequencies of values that fall in each interval.

The blue line shows the frequencies of π , the orange line the frequencies of $\hat{\pi}$ for $p \approx 0.4$, the gray line $\hat{\pi}$ for $p \approx 0.6$ and the yellow line $\hat{\pi}$ for $p \approx 0.8$. The values of p are approximate due to rescaling. In general, lower values of p offer more privacy, at the cost of less accuracy.

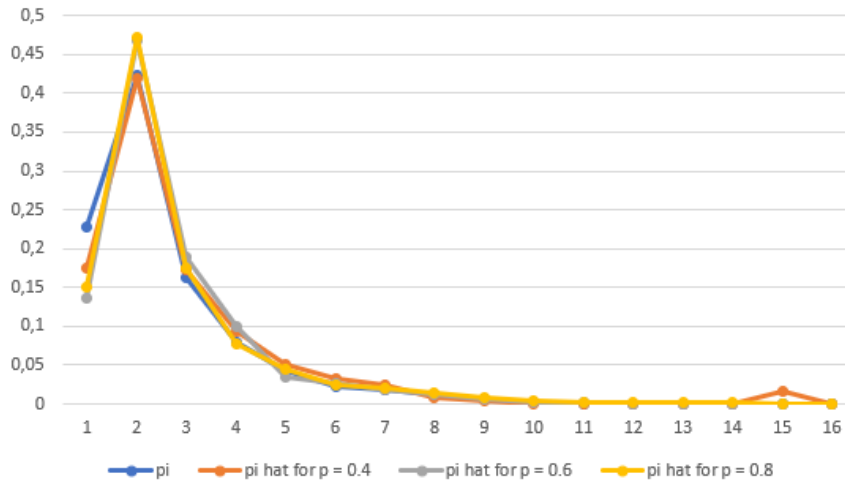


Fig. 2: Attenuation A. Original frequencies and $\hat{\pi}$ frequencies for $p = 0.4, 0.6$ and 0.8

References

- [1] J. Domingo-Ferrer and J. Soria-Comas. Connecting randomized response, post-randomization, differential privacy and t-closeness via deniability and permutation. *CoRR*, abs/1803.02139, 2018.
- [2] Z. Erkin and G. Tsudik. Private computation of spatial and temporal power consumption with smart meters. In F. Bao, P. Samarati, and J. Zhou, editors, *Applied Cryptography and Network Security*, pages 561–577, 2012. Springer.
- [3] T. Ryberg. *Smart Metering in Europe*, Berg Insight’s M2M Research Series, Nov. 2018. <http://www.berginsight.com/ReportPDF/ProductSheet/bi-sm14-ps.pdf>, accessed 2019-04-22
- [4] S. L. Warner. Randomized response: A survey technique for eliminating evasive answer bias. *Journal of the American Statistical Association*, 60(309):63–69, 1965.

This book of proceedings gathers the contributions presented at the 6th URV Doctoral Workshop in Computer Science and Mathematics. The main aim of this workshop is to promote the dissemination of the ideas, methods and results that are developed in the Doctoral Thesis of the students of this doctorate program, and to promote the knowledge sharing, collaboration and discussion between their respective research groups.

Departament d'Enginyeria



**Informàtica i
Matemàtiques**



UNIVERSITAT
ROVIRA I VIRGILI



ESCOLA TÈCNICA SUPERIOR
D'ENGINYERIA
Universitat Rovira i Virgili

